Lecture “Solid-State NMR Spectroscopy“
for PhD seminars of the graduate college GRK 448
"Modern Methods of Magnetic Resonance in Materials Sciences"
by apl. Prof. Dr. Michael Hunger

https://michael-hunger.de

Contents

Solid-state NMR spectroscopy: Hamiltonians

Hamiltonians: $$\boldsymbol{H}_{total} = \boldsymbol{H}_0 + \boldsymbol{H}_{CS} + \boldsymbol{H}_{DI} + \boldsymbol{H}_Q + \boldsymbol{H}_K + \boldsymbol{H}_J \quad (1)$$

$\boldsymbol{H}_0$:	Zeeman interaction $\gamma \cdot \hbar \cdot I_z \cdot B_0$ of nuclear spins I in the external magnetic field B_0	$\leq 10^9$ s^{-1}
$\boldsymbol{H}_{CS}$:	chemical shielding interaction caused by the electrons surrounding the nuclei	$\leq 5 \times 10^3$ s^{-1}
$\boldsymbol{H}_{DI}$:	dipolar interaction with magnetic dipoles of other nuclei in the local structure	$\leq 5 \times 10^4$ s^{-1}
$\boldsymbol{H}_Q$:	quadrupolar interaction of the electric quadrupole moment with the electric field gradient	$\leq 10^7$ s^{-1}
$\boldsymbol{H}_K$:	Knight shift due to the Fermi contact interaction between the nuclei and conduction electrons	$\leq 10^5$ s^{-1}
$\boldsymbol{H}_J$:	indirect nuclear-nuclear coupling by simultaneous coupling of the electrons	$\leq 10^3$ s^{-1}

In most applications of solid-state NMR spectroscopy, $\boldsymbol{H}_J$ is neglected since this splitting is overlapped by the stronger solid-state interactions

Generally, the Hamiltonians $\boldsymbol{H}_\lambda$ can be written in the form:

$$\boldsymbol{H}_\lambda = C_\lambda \sum_{\alpha,\beta=x,y,z} I_\alpha \cdot R_{\alpha\beta}{}^{\lambda} \cdot A_\beta \quad (2)$$

where I and A are vectors of the nuclear spin and, e.g., of the magnetic field, while $R_{\alpha\beta}{}^{\lambda}$ is a second rank tensor describing the interaction and C_λ is a typical constant of each interaction λ:

$$\boldsymbol{H}_\lambda = C_\lambda \cdot [I_x, I_y, I_z] \begin{bmatrix} R_{xx} & R_{xy} & R_{xz} \\ R_{yx} & R_{yy} & R_{yz} \\ R_{zx} & R_{zy} & R_{zz} \end{bmatrix} \begin{bmatrix} A_x \\ A_y \\ A_z \end{bmatrix} \quad (3)$$

In the principal axis system (PAS) of the microscopic unit, the tensor $R_{\alpha\beta}{}^{\lambda}$ consists of diagonal elements only. All other elements vanish.

Solid-state NMR spectroscopy: Hamiltonians

Another way to describe the Hamiltonians in the principal axis system of the microscopic unit is [Freude1]:

$$\boldsymbol{H}_\lambda = \mathrm{C}_\lambda \sum_{k=0}^{2} \sum_{q=-k}^{+k} (-1)^q T_{kq} V_{k-q} \qquad (4)$$

with the irreducible spherical tensors T_{kq} (spin term) and V_{kq} (local term). In Table 1, the operators of the Hamiltonians $\boldsymbol{H}_{CS}$, $\boldsymbol{H}_{DI}$, $\boldsymbol{H}_{Q}$ are summarized.

Table 1
Elements of the irreducible spherical tensors T_{kq} and V_{kq} of the Hamiltonians $\boldsymbol{H}_\lambda$ (λ = CS, DI, Q) in the principal axis system (PAS) [Freude1].

interaction/ parameter	chemical shielding interaction, $\boldsymbol{H}_{CS}$	homonuclear dipolar interaction*, $\boldsymbol{H}_{DI}$	quadrupolar interaction, $\boldsymbol{H}_{Q}$
C_λ	$\gamma \hbar$	$-2\gamma_i\gamma_k\hbar^2 \frac{\mu_0}{4\pi}$	$\frac{eQ}{2I(2I-1)}$
T_{20}	$\sqrt{\frac{2}{3}} I_z B_0$	$\sqrt{\frac{1}{6}} (3I_{zi}I_{zk} - I_iI_k)$	$\sqrt{\frac{1}{6}} [3I_z^2 - I(I+1)]$
$T_{2\pm1}$	$\sqrt{\frac{1}{2}} I_\pm B_0$	$\sqrt{\frac{1}{2}} (3I_{\pm i}I_{zk} - I_{zi}I_{\pm k})$	$\sqrt{\frac{1}{2}} (I_\pm I_z - I_{-z}I_\pm)$
$T_{2\pm2}$	0	$I_{\pm i}I_{\pm k}$	$I_\pm^2$
V_{20}	$\sqrt{\frac{3}{2}}(\sigma_{zz} - \sigma_{iso})$	$\sqrt{\frac{3}{2}} r_{ik}^{-3}$	$\sqrt{\frac{3}{2}} V_{zz} = \sqrt{\frac{3}{2}} eq$
$V_{2\pm1}$	0	0	0
$V_{2\pm2}$	$\frac{1}{2}(\sigma_{xx} - \sigma_{yy})$	0	$\frac{1}{2}(V_{xx} - V_{yy})$

*) for heteronuclear dipolar interactions, T_{20} must be substituted by $\sqrt{\frac{1}{6}} I_{zi}I_{zk}$

If the Hamiltonian is given by $\boldsymbol{H}_\lambda = \boldsymbol{H}_\lambda' + \boldsymbol{H}_\lambda''$ with $[\boldsymbol{H}_0, \boldsymbol{H}_\lambda'] = 0$ and $[\boldsymbol{H}_0, \boldsymbol{H}_\lambda''] \neq 0$, then $\boldsymbol{H}_\lambda'$ is the secular part.

Generally, the secular part is used to describe the NMR line shapes. In this case, only the tensor elements with $k = 2$ and $q = 0$ in Table 1 have to be considered.

Solid-state NMR spectroscopy: Hamiltonians

The tensors V'_{kq} (local term) in the laboratory axis system (LAB) are related to V_{kq} in the principal axis frame by the Wigner rotation matrices $D^{l}_{m',m}(R)$:

$$V'_{kq} = \sum_{q'=-k}^{+k} D^{k}_{q',q}(R)\, V_{kq} \qquad (5)$$

where $D^{k}_{q',q}(R)$ denote matrix elements of three-dimensional rotations.

The matrix elements $D^{k}_{q',q}(R)$ can be written as:

$$D^{k}_{q',q}(\alpha, \beta, \gamma) = \exp\{i\alpha q'\}\, d^{k}_{q',q}(\beta) \exp\{i\gamma q\} \qquad (6)$$

with the Euler angles α, β and γ (see [Rose1]).

The elements $d^{k}_{q',q}(\beta)$ of the reduced Wigner matrices depend on the angle β only.

Table 2 gives components of V'_{kq}, which were transformed from the principal axis system (PAS) into the laboratory axis system (LAB) by the Euler angles α and β via equation (6).

Table 2
Elements of the irreducible spherical tensor V'_{kq} for the different Hamiltonians $\boldsymbol{H}_{\lambda}$ (λ = CS, DI, Q) transformed into the laboratory axis system (LAB) [Freude1].

interaction/ element	chemical shielding interaction	homonuclear dipolar interaction between I_i and I_k*	quadrupolar interaction
V'_{20}	$\sqrt{\frac{3}{2}}(\sigma_{zz} - \sigma_{iso})\, F(\alpha,\beta,\eta)$	$\sqrt{\frac{3}{2}}\frac{1}{r_{ik}^3}\left(\frac{3\cos^2\beta_{ik} - 1}{2}\right)$	$\sqrt{\frac{3}{2}}\, eq \cdot F(\alpha,\beta,\eta)$

with: $$F(\alpha,\beta,\eta) = \left(\frac{3\cos^2\beta - 1}{2} + \frac{\eta}{2}\sin^2\beta\cos 2\alpha\right) \qquad (7)$$

and $$\eta = \frac{\sigma_{xx} - \sigma_{yy}}{\sigma_{zz} - \sigma_{iso}}$$ (asymmetry parameter of the chemical shielding interaction) (8)

or $$\eta = \frac{V_{xx} - V_{yy}}{V_{zz}}$$ (asymmetry parameter of the quadrupolar interaction) (9)

Solid-state NMR spectroscopy: Chemical shielding interaction

In the principal axis system (PAS), the Hamiltonian of the chemical shielding interaction is given by:

$$\boldsymbol{H}_{CS} = \gamma \cdot \hbar \cdot I \cdot \sigma_{\alpha\beta} \cdot B_0 \qquad (10)$$

with the shielding tensor $\sigma_{\alpha\beta}$.

In the PAS, the shielding tensor is reduced to its diagonal elements σ_{xx}, σ_{yy} and σ_{zz} with $|\sigma_{zz}| \geq |\sigma_{yy}| \geq |\sigma_{xx}|$.

The shift of the resonance frequency in the field B_0 is due to the σ'_{zz} component in the laboratory frame (LAB).

A rotational transformation with the Euler angles α and β leads to:

$$\sigma'_{zz} = \sigma_{xx} \sin^2\beta\cos^2\alpha + \sigma_{yy} \sin^2\beta\sin^2\alpha + \sigma_{zz} \cos^2\beta \qquad (11)$$

It is convenient to introduce the isotropic part σ_{iso}, the shielding anisotropy $\Delta\sigma$ and the asymmetry parameter η (see also eq. (8)):

$$\sigma_{iso} = \frac{1}{3}(\sigma_{xx} + \sigma_{yy} + \sigma_{zz}) \qquad (12)$$

$$\Delta\sigma = (\sigma_{zz} - \sigma_{iso}) \qquad (13)$$

$$\eta = \frac{(\sigma_{yy} - \sigma_{xx})}{\Delta\sigma} \qquad (14)$$

Transformation of the Hamiltonian into the LAB leads to:

$$\boldsymbol{H}_{CS} = \gamma \cdot \hbar \cdot I_z \cdot B_0 \left[\sigma_{iso} + \Delta\sigma \left(\frac{3\cos^2\beta - 1}{2} + \frac{\eta}{2} \sin^2\beta \cos 2\alpha \right) \right] \qquad (15)$$

corresponding to a resonance frequency ω of:

$$\omega = \omega_0 \left[(1 - \sigma_{iso}) - \Delta\sigma \left(\frac{3\cos^2\beta - 1}{2} + \frac{\eta}{2} \sin^2\beta \cos 2\alpha \right) \right] \qquad (16)$$

Solid-state NMR spectroscopy: Chemical shielding interaction

In a liquid sample, the rapid molecular reorientation averages to zero the angle-dependent terms in equation (16) and for ω follows:

$$\omega = \omega_0(1 - \sigma_{iso}) \tag{17}$$

For a polycrystalline sample, the Euler angles α and β vary from crystallite to crystallite and the resonance frequency ranges from $\omega_1 = \omega_0(1 - \sigma_{iso} - \Delta\sigma)$ to $\omega_3 = \omega_0[1 - \sigma_{iso} + (\Delta\sigma/2)(1+\eta)]$ in Figure 1.

Typically observed line shapes are given in Figure 1 for the general case (left) and for the case of an axial symmetry, i.e., $\eta = 0$ (right).

In the latter case, often following assignments are used:

$$\sigma_{\perp} = \sigma_{zz} \tag{18}$$

$$\sigma_{\parallel} = \sigma_{xx} = \sigma_{yy} \tag{19}$$

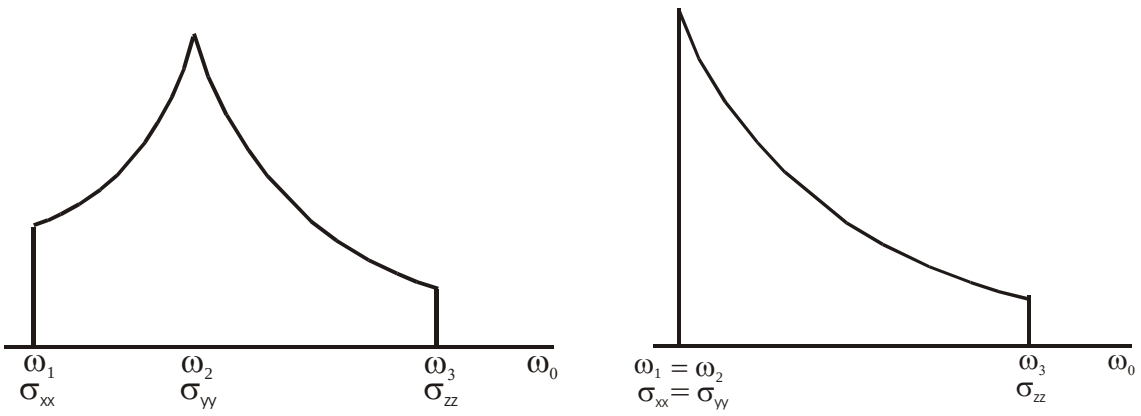

Figure 1
Line shapes of powders samples caused by chemical shielding interaction, general case (left) and axial symmetry (right).

Solid-state NMR spectroscopy: Dipolar interaction

In the laboratory frame, the Hamiltonians of dipolar interactions are given by (see Tables 1 and 2):

a) Homonuclear dipolar interaction ($\gamma_i = \gamma_k$)

$$\boldsymbol{H}_{\text{homo.DI}} = \gamma_i \gamma_k \hbar^2 \frac{\mu_0}{4\pi} \frac{1}{r_{ik}^3} \left(\frac{1 - 3\cos^2 \beta_{ik}}{2} \right) (3 I_{zi} I_{zk} - I_i I_k) \tag{20}$$

b) Heteronuclear dipolar interaction

$$\boldsymbol{H}_{\text{hetero.DI}} = \gamma_i \gamma_k \hbar^2 \frac{\mu_0}{4\pi} \frac{1}{r_{ik}^3} \left(\frac{1 - 3\cos^2 \beta_{ik}}{2} \right) I_{zi} I_{zk} \tag{21}$$

By using the raising and lowering operators $I_+ = I_x + \mathrm{i} I_y$ and $I_- = I_x - \mathrm{i} I_y$, the Hamiltonian can be written:

$$\boldsymbol{H}_{\text{DI}} = \gamma_i \gamma_k \hbar^2 \frac{\mu_0}{4\pi} \frac{1}{r_{ik}^3} \left(1 - 3\cos^2 \beta_{ik}\right) [I_{zi} I_{zk} - \frac{1}{4} (I_{+i} I_{-k} + I_{-i} I_{+k})] \tag{22}$$

With

$$\omega_{\text{DI}} = (\gamma_i \gamma_k \hbar \frac{\mu_0}{4\pi}) / r_{ik}^3 \tag{23}$$

and

$$A = (1 - 3\cos^2 \beta_{ik}) I_{zi} I_{zk} \tag{24}$$

$$B = -\frac{1}{4} (1 - 3\cos^2 \beta_{ik}) [I_{+i} I_{-k} + I_{-i} I_{+k}] \tag{25}$$

follows

$$\boldsymbol{H}_{\text{DI}} = \hbar \, \omega_{\text{DI}} (A + B) \tag{26}$$

Term A is the so-called static part, which describes the modification of the value of B_0 at the sites of the resonating nuclei and causes the dispersion of the Zeeman levels and Larmor frequencies.

Term B is called flip-flop term and describes the polarization transfer between neighboring spins, also called spin diffusion.

For a heteronuclear coupling, the Zeeman levels are not equidistant and, therefore, term B vanishes.

Solid-state NMR spectroscopy: Dipolar interaction

Spectra due to the dipolar coupling of isolated spin pairs with I = ½ consist of two subspectra with inverse signs, corresponding to the two transitions with $\Delta m = \pm 1$.

For a homonuclear dipolar coupling, two absorption lines (fixed angle β_{ik}) occur at the frequencies (see Fig. 2, left):

$$\omega_1 = \omega_0 - \frac{3}{4}\omega_{DI}(1-3\cos^2\beta_{ik}) \quad (27)$$

and

$$\omega_2 = \omega_0 + \frac{3}{4}\omega_{DI}(1-3\cos^2\beta_{ik}) \quad (28)$$

For heteronuclear dipolar coupling, term B (eq. (25)) disappears and the lines occur at:

$$\omega_1 = \omega_0 - \frac{1}{2}\omega_{DI}(1-3\cos^2\beta_{ik}) \quad (29)$$

and

$$\omega_2 = \omega_0 + \frac{1}{2}\omega_{DI}(1-3\cos^2\beta_{ik}) \quad (30)$$

In the case of a powder, the different angles β_{ik} of the spin pairs in different crystallites cause patterns as shown in Figure 2, right:

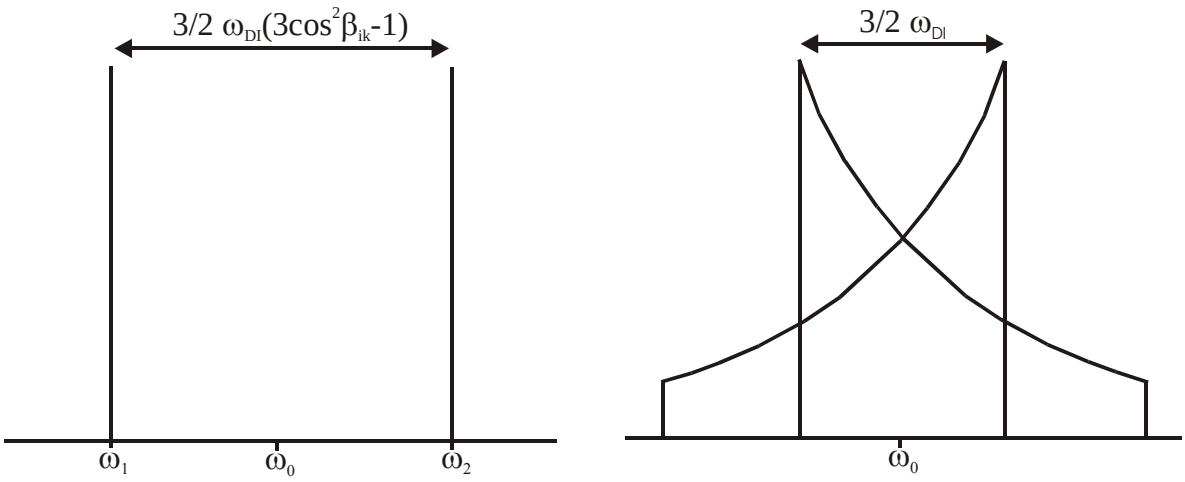

Figure 2
Theoretical spectra caused by pairs of homonuclear spins in a single crystal (left) and in a powder (right).

Solid-state NMR spectroscopy: Quadrupolar interaction

About 100 isotopes exhibit a nuclear spin $I > ½$, i.e., are quadrupolar nuclei.

For nuclei with spin $I > ½$, the electric charge distribution $\rho(r)$ in the nucleus is not spherical and causes an electric quadrupole moment eQ [Fraiss1]:

$$eQ = \int \rho(r)\, r^2\, (3\cos^2\Theta - 1)\, \mathrm{d}v \qquad (31)$$

where the integration is taken over the whole space of which dv is the volume element.

In this case, to the orientation of the magnetic moment μ in B_0 is added the orientation energy E_Q of the electric quadrupole moment eQ in the electric field related to the distribution of charges in the local structure:

$$E_Q = \int \rho(\mathrm{r})\, V(\mathrm{r})\, \mathrm{d}v \qquad (32)$$

with the potential V(r) of the electric field. The electric field gradient is a traceless second rank tensor:

$$V_{ij} = \frac{\partial^2 V}{\partial i \partial j} \quad \text{with} \quad i, j = x,y,z \qquad (33)$$

In the principal axis system, the electric field gradient V_{ij} is diagonal with $|V_{zz}| \geq |V_{yy}| \geq |V_{xx}|$ and $V_{zz} = eq$.

According to Tables 1 and 2, the Hamiltonian $\boldsymbol{H}_Q$ of the quadrupolar interaction is:

$$\boldsymbol{H}_Q = \frac{e^2 qQ}{4I(2I-1)}[3I_z^2 - I(I+1)]\left(\frac{3\cos^2\beta - 1}{2} + \frac{\eta}{2}\sin^2\beta\cos 2\alpha\right) \qquad (34)$$

The asymmetry parameter η of the electric field gradient is given by equation (9).

Commonly, the quadruple coupling constant C_{qcc} (also C_q or QCC) is given by:

$$C_{qcc} = \frac{e^2 qQ}{h} \qquad (35)$$

Solid-state NMR spectroscopy: Quadrupolar interaction

while the quadrupole frequency is defined by:

$$\nu_Q = \omega_Q / 2\pi = \frac{3e^2qQ}{2I(2I-1)h} = \frac{3C_{qcc}}{2I(2I-1)} \quad (36)$$

If $\boldsymbol{H}_Q << \boldsymbol{H}_0$ and at high field, the quadrupolar interaction is treated as a perturbation.

The first order perturbation energy $E_m^{(1)}$ is:

$$E_m^{(1)} = \frac{1}{6}\omega_Q(3\cos^2\beta\text{-}1)[3m^2\text{-}I(I\text{+}1)] \quad (37)$$

The energy difference between states m-1 and m gives the resonance frequencies:

$$\omega_m^{(1)} = \omega_0 + \frac{1}{2}\omega_Q(3\cos^2\beta\text{-}1)(1\text{-}2m) \quad (38)$$

In the case of m = ½, which corresponds to the central transition, follows $\omega_m^{(1)} = \omega_0$.

Hence, the first order perturbation term describes the splitting into central and satellite transitions as illustrated for a spin I = 3/2 system in Figure 3.

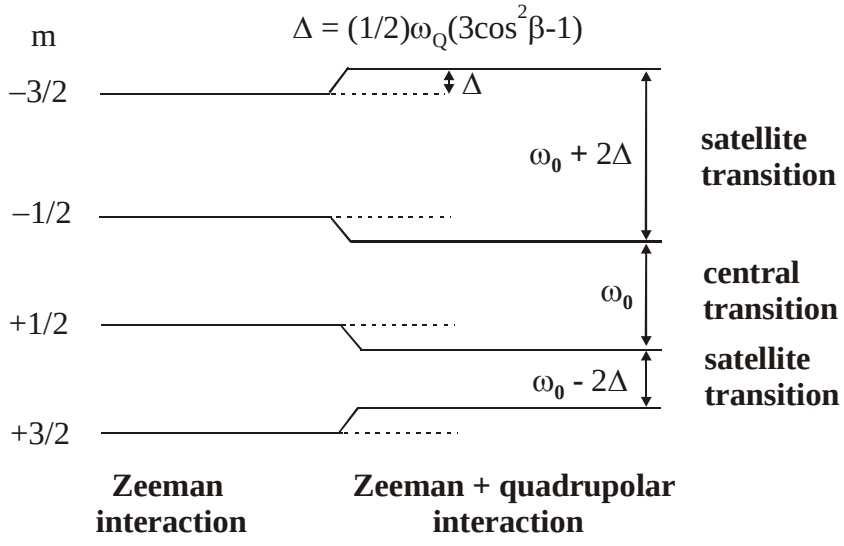

Figure 3
Level scheme of a spin I = 3/2 system with quadrupolar interaction.

Solid-state NMR spectroscopy: Quadrupolar interaction

The spectra resulting for spin I = 3/2 involved in quadrupolar interactions are given in Figure 4.

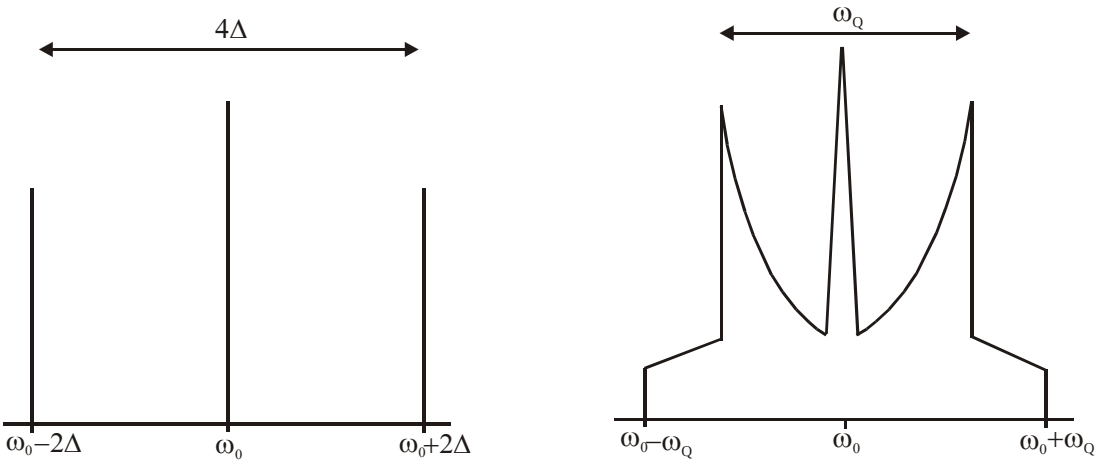

Figure 4
Theoretical spectra of a spin I = 3/2 system with quadrupolar interaction in a single crystal (left) and a powder (right).

The relative intensities of the central transitions (CT) and satellite transitions (ST) of nuclei involved in quadrupolar interactions are given by:

$$I(\mathrm{CT,ST}) = \frac{3}{2}\frac{I(I+1)-m(m-1)}{I(I+1)(2I+1)} \qquad (39)$$

Relative intensities I(CT,ST) of spin I = 1 to I = 5/2 systems:

Transition type:	**ST**	**ST**	**ST**	**ST**	**CT**	**ST**	**ST**	**ST**	**ST**
I = 1				1/2		1/2			
I = 3/2			3/10		4/10		3/10		
I = 2		2/10		3/10		3/10		2/10	
I = 5/2	5/35		8/35		9/35		8/35		5/35

In the cases of I = 1 and I = 2, no central transition occurs.

Solid-state NMR spectroscopy: Quadrupolar interaction

The first-order and second-order Hamiltonians are given by equations (40) and (41):

$$\boldsymbol{H}_{\mathrm{Q}}^{(1)} = \frac{h\omega_Q}{6}[3I_z^2 - I(I+1)] \tag{40}$$

$$\boldsymbol{H}_{\mathrm{Q}}^{(2)} = \frac{h\omega_Q^2}{9\omega_0}\left[2I_z\left(2I_z^2 - I(I+1) + \frac{1}{4}\right)V_{2-1}V_{21} + I_z\left(I_z^2 - I(I+1) + \frac{1}{2}\right)V_{2-2}V_{22}\right] \tag{41}$$

with the tensor elements V_{2k} in Table 1 (Freude1). The second-order frequency functions are given by equations (42) and (43):

$$\omega_{\mathrm{m,m+1}}^{(2)} = -\frac{\omega_Q^2}{18\omega_0}\{[24m(m+1)-4I(I+1)+9]V_{21}V_{2-1} + [6m(m+1)-2I(I+1)+3]V_{22}V_{2-2}\} \tag{42}$$

$$\omega_{\mathrm{m,-m}}^{(2)} = -\frac{m\omega_Q^2}{18\omega_0}\{[4I(I+1)-8m^2-1]V_{21}V_{2-1} + [2I(I+1)-2m^2-1]V_{22}V_{2-2}\} \tag{43}$$

for single and symmetric quantum transitions, respectively.

In the laboratory frame and in the case of the central transition ($m = -1/2 \leftrightarrow m = +1/2$), the second-order frequency function $\omega_{-1/2,1/2}^{(2)}$ is [Freude1]:

$$\omega_{-1/2,1/2}^{(2)} = -\frac{\omega_Q^2}{6\omega_0}\left[I(I+1) - \frac{3}{4}\right](\mathrm{A}\cos^4\beta + \mathrm{B}\cos^2\beta + \mathrm{C}) \tag{44}$$

with

$$\mathrm{A} = -\frac{27}{8} - \frac{9}{4}\eta\cos 2\alpha - \frac{3}{8}\eta^2\cos^2 2\alpha \tag{45}$$

$$\mathrm{B} = +\frac{15}{4} - \frac{1}{2}\eta^2 + 2\eta\cos 2\alpha + \frac{3}{4}\eta^2\cos^2 2\alpha \tag{46}$$

$$\mathrm{C} = -\frac{3}{8} + \frac{1}{3}\eta^2 + \frac{1}{4}\eta\cos 2\alpha - \frac{3}{8}\eta^2\cos^2 2\alpha \tag{47}$$

Solid-state NMR spectroscopy: Quadrupolar interaction

Equation (44) allows the calculation of the field-dependent second-order quadrupolar frequency shift ν_{qs} of the center of gravity ν_{cg} of the central transition in relation to the resonance position observed without quadrupolar interaction:

$$\nu_{qs} = \nu_{cg} - \nu_0 (1-\sigma)$$

$$= -\frac{1}{30}\frac{\nu_Q^2}{\nu_0}\left[I(I+1)-\frac{3}{4}\right](1+\frac{1}{3}\eta^2) \qquad (48)$$

The difference $\Delta\nu$ between the center of gravity of the satellite transitions (mean resonance position of the first satellites) and of the central transition is given by [Freude1]:

$$\Delta\nu = -\frac{\nu_Q^2}{30\nu_0}9\left(1+\frac{\eta^2}{3}\right) \qquad (49)$$

Hence, there are four methods to determine ν_Q:

1) In the case of weak quadrupolar interaction, the distance of the singularities of the satellite transitions are evaluated or simulated.

2) In the case of strong quadrupolar interaction, the shape in the central transition is simulated.

3) The field-dependent second-order shift is evaluated.

4) The difference between the centers of gravity of the satellite transitions (average resonance position of the first satellites) and of the central transition is evaluated.

Solid-state NMR spectroscopy: Knight shift

In metals and metallic particles, the spins of conduction electrons with ‘s’-character are polarized by B_0 and give rise to an additional shift. This shift is due to the Fermi contact interaction of the conduction electrons with the nuclear spins.

The contact interaction results in an isotropic hyperfine interaction constant [Fraiss1]:

$$a = \frac{8\pi}{3}\gamma_e\gamma_n\hbar\left\langle|\Psi(0)|^2\right\rangle_F \tag{50}$$

where $\left\langle|\Psi(0)|^2\right\rangle_F$ denotes the average density of the conduction electron wave function with the energy E_F at the nuclear position.

Due to high mobility of the conduction electrons, an average value of all hyperfine splittings is observed, leading to the relative shift $\Delta\nu$ or Knight shift K:

$$K = \frac{\Delta\nu}{\nu_0} = \frac{a\cdot\chi_P}{\gamma_e\gamma_n\hbar} \tag{51}$$

with the Pauli susceptibility χ_P of the conduction electrons and the gyromagnetic ratios γ_e and γ_n of the electrons and the coupled nuclei, respectively.

The temperature dependence of the Knight shift is given by the Korringa relation:

$$K^2 = \frac{\hbar}{4\pi k_B}\left(\frac{\gamma_e}{\gamma_n}\right)^2 S\frac{1}{T_1T} \tag{52}$$

with the spin-lattice relaxation time T_1, the temperature T, and the scaling factor S, which has the value 1 for non-interacting electrons in a three-dimensional system (not on a surface!).

The Knight shift K is orders of magnitude larger than the chemical shielding σ_{iso} and has normally a positive sign:

$$\omega = \omega_0(1 - \sigma_{iso} + K) \tag{53}$$

The Hamiltonian $\boldsymbol{H}_K$ is given by:

$$\boldsymbol{H}_K = \gamma\cdot\hbar\cdot\boldsymbol{K}\cdot\boldsymbol{I}\cdot\boldsymbol{B}_0 \tag{54}$$

Solid-state NMR spectroscopy: The method of moments

An important approach to evaluate the shapes of solid-state NMR signals is the method of moments.

According to van Vleck, the free induction decay $G(t)$ can be described by a Taylor evolution of the moments M_n [Abra1]:

$$G(t) = \sum_{n=0}^{\infty} \frac{(-i \cdot t)^n}{n!} M_n \tag{55}$$

with the n-th moment

$$M_n = \frac{\int_{-\infty}^{+\infty} (\omega - \omega_0)^n g(\omega - \omega_0) d(\omega - \omega_0)}{\int_{-\infty}^{+\infty} g(\omega - \omega_0) d(\omega - \omega_0)} \tag{56}$$

and the frequency function $g(\omega\text{-}\omega_0)$ describing the intensity distribution. Since in the most cases, the odd-numbered moments vanish, $G(t)$ follows to:

$$G(t) = 1 - \frac{M_2}{2!} t^2 + \frac{M_4}{4!} t^4 ..... \tag{57}$$

Using equation (55), the even-numbered moments can be determined:

$$M_{2n} = (-1)^n \frac{d^{2n}}{dt^{2n}} G(t)_{t=0} \tag{58}$$

According to equation (56), the second moment can be obtained by an evaluation of the spectrum using:

$$M_2 = \int_{-\infty}^{+\infty} (\omega - \omega_0)^2 g(\omega - \omega_0) d(\omega - \omega_0) \tag{59}$$

For Gaussian line shapes, also the full line width at half amplitude $\Delta\nu_{1/2}$ can be used to determine the second moment M_2:

$$\Delta\nu_{1/2} = \frac{1}{\pi} \sqrt{2 \ln 2} \sqrt{M_2} \tag{60}$$

$$M_2 = \frac{\pi^2 \Delta\nu_{1/2}^2}{2\ln 2} \tag{61}$$

Solid-state NMR spectroscopy: The method of moments

Considering the signal shapes in Figures 1 and 2 with $\Delta\omega_{CS} = \omega_3 - \omega_1$ and $\Delta\omega_{DI} = \frac{3}{2}\omega_{DI}$, the second moments of the chemical shielding interaction and the dipolar interaction, respectively, are given by:

$$M_{2,\mathrm{CS}} = \frac{4}{9}\frac{(\Delta\omega_{CS})^2}{5}\left(1+\frac{\eta^2}{3}\right) \tag{62}$$

and

$$M_{2,\mathrm{DI}} = \frac{\Delta\omega_{DI}^2}{5} \tag{63}$$

For a signal broadening by a quadrupolar interaction, the second moment of the central transition is given by:

$$M_2 = \frac{23}{7}\nu_{qs}^2 \tag{64}$$

with

$$\nu_{\mathrm{qs}} = -\left(\frac{\nu_Q^2}{30\nu_0}\left[I(I+1)-\frac{3}{4}\right]\left(1+\frac{\eta^2}{3}\right)\right) \tag{65}$$

A more general approach is to calculate the second moment via the Hamiltonian $\boldsymbol{H}_\lambda$ of the interaction λ under study according to:

$$M_2 = \frac{Tr\left\{\left[H_\lambda, I_y\right]^2\right\}}{Tr\left\{I_x^2\right\}} \tag{66}$$

For the secular part of the homonuclear dipolar interaction follows:

$$M_{2,\mathrm{II}} = 3\gamma_I^4\hbar^2 I(I+1)\left(\frac{\mu_0}{4\pi}\right)^2 \frac{1}{N}\sum_{i=1}^{N}\sum_{k\neq i}^{N}\left(\frac{1-3\cos^2\beta_{ik}}{2}\right)^2 \frac{1}{r_{ik}^6} \tag{67}$$

Solid-state NMR spectroscopy: The method of moments

For the secular part of the heteronuclear dipolar interaction follows:

$$M_{2,\mathrm{IS}} = \frac{3}{4}\gamma_I^2\gamma_S^2\hbar^2 S(S+1)\left(\frac{\mu_0}{4\pi}\right)^2 \frac{1}{N}\sum_{i=1}^{N}\sum_{k=1}^{N}\left(\frac{1-3\cos^2\beta_{ik}}{2}\right)^2 \frac{1}{r_{ik}^6} \tag{68}$$

with the powder average:

$$\left\langle\left(\frac{1-3\cos^2\beta_{ik}}{2}\right)^2\right\rangle_{powder} = \frac{1}{5} \tag{69}$$

In the following, a simple approach for calculating the second moment of powder signals broadened by dipolar interactions is demonstrated. Generally, the second moment M_2 due to dipolar interactions of an ensemble of I and S spins is the sum of the homonuclear term $M_{2,\mathrm{II}}$ and the heteronuclear term $M_{2,\mathrm{IS}}$, which can be described by:

$$M_2 = \frac{C_I}{r_I^6} + \frac{C_S}{r_S^6} \tag{70}$$

with

$$C_\mathrm{I} = \frac{3}{5}I(I+1)\left(\frac{\mu_0}{4\pi}\right)^2 \gamma_I^2\hbar^2 \quad (\cdot 10^{68}) \tag{71}$$

$$C_\mathrm{S} = \frac{4}{15}S(S+1)\left(\frac{\mu_0}{4\pi}\right)^2 \gamma_S^2\hbar^2 \quad (\cdot 10^{68}) \tag{72}$$

The factor 10^{68} is valid for M_2 values given in 10^{-8} T^2 and r in Å and:

$$\frac{1}{r_I^6} = \frac{1}{N}\sum_{i=1}^{N}\sum_{k\neq i}^{N}\frac{1}{r_{ik}^6} \tag{73}$$

$$\frac{1}{r_S^6} = \frac{1}{N}\sum_{i=1}^{N}\sum_{k=1}^{N}\frac{1}{r_{ik}^6} \tag{74}$$

Comparison of equations (69) and (70) leads to:

$$C_\mathrm{S} = \frac{4}{9}\cdot C_\mathrm{I} \tag{75}$$

Solid-state NMR spectroscopy: The method of moments

The value C_I of the nucleus X can be calculated by:

$$C_I(X) = C_I(^1H)\ \frac{I(I+1)}{\frac{3}{4}}\ \frac{\nu_0(X)^2}{\nu_0(^1H)^2} \tag{76}$$

with $C_I(^1H) = 358.1$ and the resonance frequencies $\nu_0(X)$ and $\nu_0(^1H)$ of the nuclei X and ^{1}H, respectively.

In a field with a ^{1}H resonance frequency of 500 MHz, e.g., the ^{13}C and the ^{27}Al resonance frequencies are 125.6 MHz and 130.3 MHz, respectively, and C_I and C_S follow to:

$$C_I(^{13}C) = 358.1\ \frac{\frac{3}{4}}{\frac{3}{4}}\left(\frac{125.6}{500}\right)^2 = 22.6 \tag{77}$$

and

$$C_S(^{13}C) = \frac{4}{9}\,22.6 = 10.0 \tag{78}$$

or

$$C_I(^{27}Al) = 358.1\ \frac{\frac{35}{4}}{\frac{3}{4}}\left(\frac{130.3}{500}\right)^2 = 283.7 \tag{79}$$

and

$$C_S(^{27}Al) = \frac{4}{9}\,283.7 = 126.1 \tag{80}$$

In the local structure of bridging OH groups (SiOHAl) in zeolites, the hydroxyl proton is involved in a heteronuclear dipolar interaction with one framework aluminium atom. This interaction is the dominating line broadening mechanism in the ^{1}H NMR spectrum.

By an evaluation of the ^{1}H NMR line width, a second moment of $M_2 = 0.7\times10^{-8}$ T^2 was determined.The second term of equation (70) yields an H-Al distance of 2.377 Å.

Solid-state NMR spectroscopy: Experimental techniques / Excitation

The radio frequency (rf) pulses applied to excite a spin system is described by:

$$\boldsymbol{H}_{\mathrm{rf}} = 2\hbar\omega_1 \cos(\omega t) I_x \qquad (81)$$

with the nutation frequency $\omega_1 = \gamma B_1$. This nutation frequency has values of 1 – 400 kHz.

Generally, the pulse length t_p is given by:

$$t_p = \frac{\alpha}{\omega_1} = \frac{\alpha}{\gamma B_1} \qquad (82a)$$

with the nutation angle $\alpha = \pi/2, \pi \ldots$. The frequency range $\Delta\nu$, which is excited by a pulse with the length t_p, amounts to:

$$\Delta\nu \approx 1/(\pi\, t_p) \qquad (82b)$$

Aluminum nuclei with a C_{qcc} value of 10 MHz, e.g., cause a ^{27}Al NMR signal with a spectral range $\Delta\nu$ of ca. 3 MHz (see eq. (36) and Fig. 4, right). The full excitation of this spectral range requires a pulse with a length of $t_p \leq 0.1$ µs!

In the case of a single $\pi/2$ pulse excitation, the repetition time t_{rep} should be ca. $5 \times T_1$. Otherwise, saturation of the magnetization occurs.

Shorter repetition times require the application of the Ernst angle α_{opt} ($\cos \alpha_{opt} = \exp\{-t_{rep}/T_1\}$, which is optimised to decrease saturation effects.

For a spin system with a T_1 time of 5 s, the following optimised nutation angles as a function of the repetition time should be used:

repetition time	7.5 s	5.0 s	2.5 s
$\boldsymbol{\alpha_{opt}}$	77°	68°	53°

Solid-state NMR spectroscopy: Experimental techniques / Excitation

For the strongest solid-state interaction causing broadest frequency distribution functions, the quadrupolar interaction, following cases have to be distinguished:

$$|\boldsymbol{H}_{rf}| > |\boldsymbol{H}_{Q}| \qquad (*)$$

and

$$|\boldsymbol{H}_{rf}| < |\boldsymbol{H}_{Q}| \qquad (**)$$

A so-called hard pulse (short duration, high power) can perform a ***nonselective excitation*** of the whole quadrupolar spectrum if the rf field strength meets (*), while a soft pulse (long duration, low power) cause a ***selective excitation*** of single transitions ($m = -I, -I+1, \ldots, I-1$) such as the central transition ($m = -1/2$).

In the case of a ***nonselective excitation*** of all transitions, the intensity of the FID $G_{m,m+1}^{nonselective}(0)$ after a pulse with the *rf* field strength ω_1 and the pulse duration t_p is [Freude2]:

$$G_{m,m+1}^{nonselective}(0) = \frac{3[I(I+1)-m(m+1)]}{2I(I+1)(2I+1)}\sin(\omega_1 t_p) \qquad (83)$$

Equation (83) gives the relative intensities of all transitions (compare eq. (39)).

The ***selective excitation*** leads to an FID of:

$$G_{m,m+1}^{selective}(0) = \frac{3\sqrt{[I(I+1)-m(m+1)]}}{2I(I+1)(2I+1)}\sin(\sqrt{[I(I+1)-m(m+1)]}\omega_1 t_p) \qquad (84)$$

Comparison of equations (83) and (84) reveals that the maximum intensity is reduced by $\sqrt{[I(I+1)-m(m+1)]}$, but the effective nutation frequency ω_1^{eff} is enhanced by the same value, i.e., for the central transition (m = -1/2) by:

$$\omega_1^{eff} = (I+\frac{1}{2})\omega_1 \qquad (85)$$

For selective excitation, therefore, the nonselective π/2 pulse devided by (I + 1/2) is the optimum pulse.

Solid-state NMR spectroscopy: Experimental techniques / CP

Investigation of nuclei with small gyromagnetic ratio and low concentration can be improved by magnetization transfer from the abundant to the rare spins using cross polarization (CP).

In the high-temperature approximation, the population differences ΔN_I and ΔN_S of spins *I* and *S* are in the ratio:

$$\frac{\Delta N_I}{\Delta N_S} = \frac{\gamma_I}{\gamma_S} \tag{86}$$

Therefore, it is interesting to transfer magnetization from the ^{1}H spins *I* to the rare spins *S* with a lower gyromagnetic ratio.

In the cross polarization experiment, the abundant and rare spins are locked in a radio frequency field applying the pulse group shown in Figure 5.

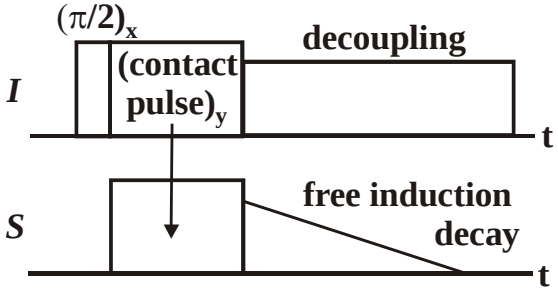

Figure 5
Pulse sequence of the cross polarization experiment.

During the contact pulse, the spins *I* toggled by the $(\pi/2)_x$ pulse to y and the spins *I* and *S* are locked along the B_1 fields (see Figure 6, left). If $\omega_{1,S} = \omega_{1,I}$ (Hartmann-Hahn condition), magnetization transfer occurs (see Figure 6, right).

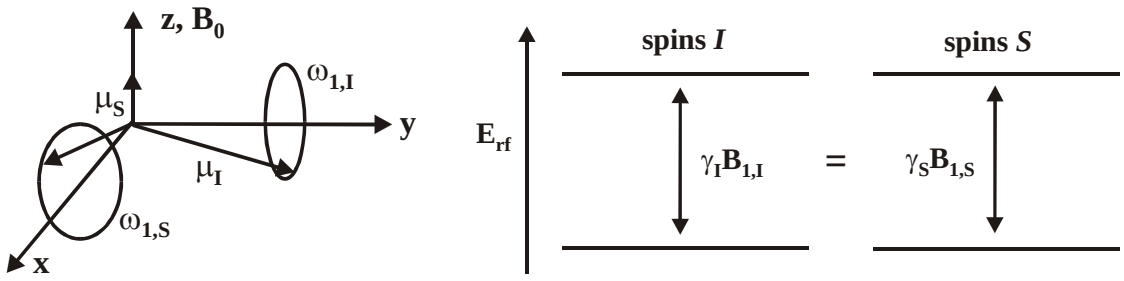

Figure 6
Spin-locking during irradiation of the contact pulse (left) and energy splitting in the rf field (right) fitting the Hartmann-Hahn condition.

Solid-state NMR spectroscopy: Experimental techniques / CP

During the spin-locking in the rf fields, relaxation occurs with the characteristic time $T_{1\rho}$, which is the T_1 time in the rotating frame.

The time dependence of the spin *S* magnetization $M_S(t)$ is plotted in Figure 7 [Michel1].

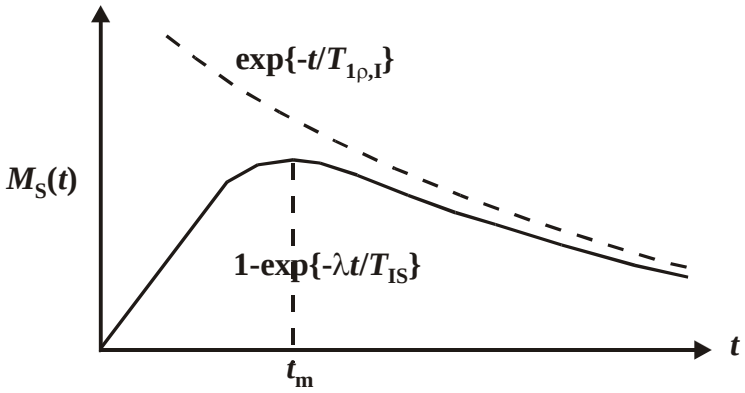

Figure 7
Time dependence of the spin *S* magnetization $M_s(t)$.

The decay of $M_s(t)$ in Figure 7 depends on the relaxation $T_{1\rho,I}$ of the spins *I* (dotted line) and the cross-polarization rate T_{IS}^{-1} given by:

$$\frac{1}{T_{IS}} = \frac{3}{2} M_{2,IS} \left(\frac{2\pi}{5 M_{2,II}} \right)^{1/2} \tag{87}$$

with the second moment of heteronuclear ($M_{2,IS}$) and homonuclear ($M_{2,II}$) dipolar interaction (see eqs. (67) and (68)).

The parameter λ in Figure 7 corresponds to:

$$\lambda = 1 + \frac{T_{IS}}{T_{1\rho,S}} - \frac{T_{IS}}{T_{1\rho,I}} \tag{88}$$

The maximum spin *S* magnetization is reached after the time t_m:

$$t_{\mathrm{m}} = \frac{T_{IS} \cdot T_{1\rho,I}}{T_{1\rho,I} - T_{IS}} \cdot \ln\left(\frac{T_{1\rho,I}}{T_{IS}}\right) \tag{89}$$

Solid-state NMR spectroscopy: Experimental techniques / MAS

The technique of magic angle spinning (MAS) consists of a mechanical rotation of the sample with a frequency ν_{rot} of up to 40 kHz

For two spins *I* and *S* connected by a vector r_{IS}, the angle β between B_0 and r_{IS} is given by (see Figure 8):

$$\cos\beta = \cos\Theta\cdot\cos\gamma + \sin\Theta\cdot\sin\gamma\cdot\cos\omega_{rot}t \qquad (90)$$

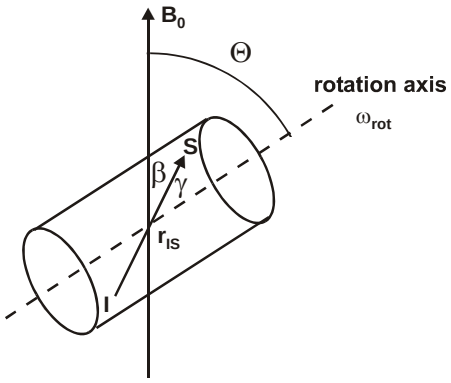

Figure 8
Under fast sample rotation, the angle β between B_0 and r_{IS} is a function of time.

With the mean values over a period $\langle\cos\omega_{rot}t\rangle = 0$ and $\langle\cos^2\omega_{rot}t\rangle = 1/2$ follows:

$$\langle 3\cos^2\beta - 1\rangle = \frac{1}{2}(3\cos^2\Theta - 1)(3\cos^2\gamma - 1) \qquad (91)$$

This term cancels, if $\Theta = 54^o\ 44'$, the so-called magic angle.

Effect of magic angle spinning on solid-state interactions exhibiting the geometric term $(3\cos^2\Theta - 1)$:

1) A homogeneous broadening is effectively reduced, if ω_{rot} is larger than the line width without rotation. In the other case, for homonuclear dipolar interaction, the flip-flop term B hinders an averaging by MAS.

2) For inhomogeneous broadening (anisotropic shielding interaction, heteronuclear dipolar interaction, quadrupolar interaction) and a rotation rate less than the anisotropy, the spectrum is reduced to its isotropic value and spinning sidebands occur at $\nu = \nu_0 \pm n \times \nu_{rot}$ with $n = 1, 2 \ldots$. There are several methods to suppress spinning sidebands by irradiating pulse sequences (e.g. TOSS [Dixon1]).

Solid-state NMR spectroscopy: Experimental techniques / MAS

For a thermal mobility of the nuclei under study with a correlation time $\tau_c < 1/\omega_{rot}$, the width of the MAS central line, $\Delta\nu_{1/2}^{MAS}$, is given by [Andrew1]:

$$\Delta\nu_{1/2}^{MAS} = \frac{1}{6\pi} M_2 \left[\frac{2\tau_c}{1+(\omega_{rot}\tau_c)^2} + \frac{\tau_c}{1+4(\omega_{rot}\tau_c)^2} \right] \qquad (92)$$

with the static second moment M_2 (see Figure 9).

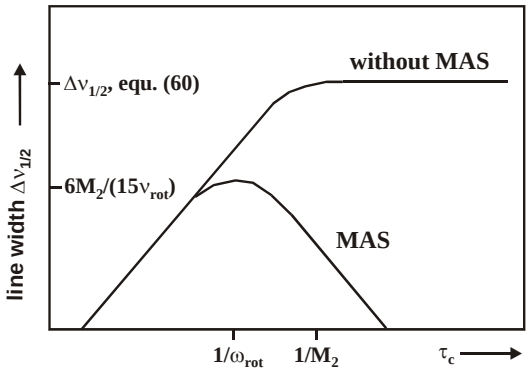

Figure 9
Line width $\Delta\nu_{1/2}$ as a function of the correlation time τ_c [Andrew1].

The influence of thermal motion on the decay $G^{MAS}(t)$ under MAS is [Pfeifer1]:

$$G^{MAS}(t) = \exp\{-(M_{2,IS}/3)[2J(\omega_{rot}, t)+J(2\omega_{rot}, t)]\} \qquad (93)$$

with

$$J(\omega_{rot}, t)) = \frac{\tau_c t}{1+(\omega_{rot}\tau_c)^2} + \frac{\tau_c^2((\omega_{rot}\tau_c)^2-1)}{(1+(\omega_{rot}\tau_c)^2)^2}(1-e^{-t/\tau_c}\cos(\omega_{rot}t)) - \frac{2\omega_{rot}\tau_c^3}{(1+(\omega_{rot}\tau_c)^2)^2} e^{-t/\tau_c}\sin(\omega_{rot}t) \qquad (94)$$

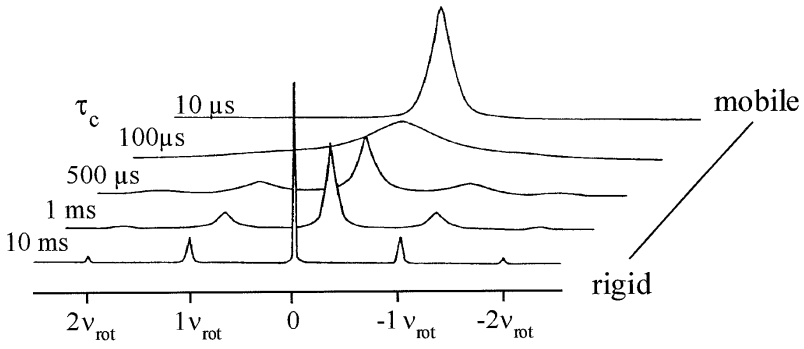

Figure 10

Calculated ^{1}H MAS NMR spectra (ν_{rot} = 3 kHz) of bridging OH groups in zeolite H-Y ($M_{2,IS} = 0.7 \times 10^{-8}$ T^2) characterized by different thermal mobilities (τ_c).

Solid-state NMR spectroscopy: Experimental techniques / MAS

The effect of MAS on quadrupolar broadening of the central transition is given by [Freude1]:

$$M_2^{\mathrm{MAS}} = \frac{1}{4}\left(\frac{\nu_Q^2}{30\nu_0}\left[I(I+1)-\frac{3}{4}\right]\left(1+\frac{\eta^2}{3}\right)\right)^2 \qquad (95)$$

or

$$M_2^{\mathrm{MAS}} = \frac{1}{4}\nu_{qs}^2 \qquad (96)$$

Hence, with equation (64) can be shown that the narrowing achieved by MAS is:

$$\sqrt{\frac{M_2^{static}}{M_2^{MAS}}} = \sqrt{\frac{92}{7}} \approx 3.6 \qquad (97)$$

This narrowing of the central transition is combined by a change in the line shape which can be described by equation (44), but modified terms A, B and C [Freude1]:

$$\mathrm{A} = +\frac{21}{16}-\frac{7}{8}\eta\cos 2\alpha-\frac{7}{48}\eta^2\cos^2 2\alpha \qquad (98)$$

$$\mathrm{B} = -\frac{9}{8}-\frac{1}{12}\eta^2+\eta\cos 2\alpha-\frac{7}{24}\eta^2\cos^2 2\alpha \qquad (99)$$

$$\mathrm{C} = +\frac{5}{16}-\frac{1}{8}\eta\cos 2\alpha+\frac{7}{48}\eta^2\cos^2 2\alpha \qquad (100)$$

with the Euler angle α and the asymmetry parameter η.

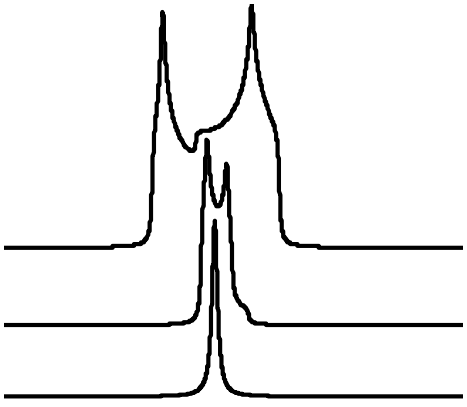

Figure 11
Line shapes of a central transition with η = 0.2, without (top) and with MAS (middle) and with DOR or MQMAS NMR (bottom).
https://michael-hunger.de

Solid-state NMR spectroscopy: Experimental techniques / Multiple-pulse sequences

In the case of strong homonuclear dipolar interactions and if anisotropy of chemical shift should be studied, averaging by multiple-pulse sequences is performed.

By toggling the magnetization with 90^o pulses along x (100), y (010) and z (001) for equal times, it is directed on average along (1,1,1) with the magic angle to the z (001) axis (see Figure 12).

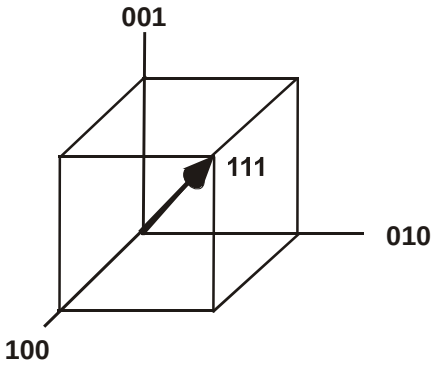

Figure 12
The angle between the diagonal (111) and each side of a cube is equal to the magic angle.

A pulse sequence to toggle the magnetization in an appropriate manner is shown in Figure 13.

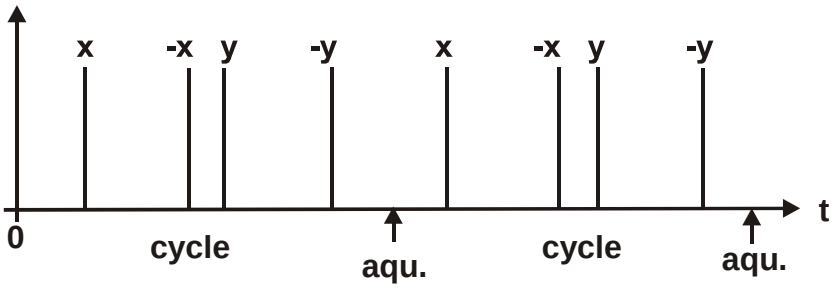

Figure 13
Multiple-pulse sequence WAHUHA4 [Fraiss1].

The whole sequence consists of a repetition of *n* elementary cycles with the cycle time t_c. At time zero, the magnetization lies along the z direction. The effect of the pulse sequence is to toggle the magnetization along the three axis. In the middle of the large window (aqu.) per cycle, a date point is sampled.

In the most cases, multiple-pulse sequences cause a scaling of the chemical shift ($1/\sqrt{3}$ for WAHUHA4) [Grimmer1].

Using the pulse operators $P_{x,y}$ and $P_{-x,-y}$:

$$P_{x,y} = \exp\left(-\frac{i}{\hbar}\frac{\pi}{2}I_{x,y}\right) \tag{101}$$

and

$$P_{-x,-y} = \exp\left(\frac{i}{\hbar}\frac{\pi}{2}I_{x,y}\right) \tag{102}$$

the pulse sequence shown in Figure 13 can be described by:

$$(\tau, P_x, 2\tau, P_{-x}, \tau, P_y, 2\tau, P_{-y}, \tau)_n \tag{103}$$

According to the concept of the time averaged Hamiltonian, the behavior of the system at times $n{\cdot}t_c$ with the number n of cycles and the cycle time t_c is given by:

$$\overline{H} = \frac{1}{t_c}\int_0^{t_c} dt' H(t') \tag{104}$$

which leads to:

$$\overline{H} = \frac{1}{3}\left(H_x + H_y + H_z\right) \tag{105}$$

The Hamiltonian of homonuclear dipolar interaction (see eq. (20)) can be written:

$$\boldsymbol{H}_z = \sum_{i\neq k} \gamma_i\gamma_k\hbar^2 \frac{\mu_0}{4\pi} \frac{1}{r_{ik}^3}\left(\frac{1-3\cos^2\Theta_{ik}}{2}\right)(3I_{zi}I_{zk} - \boldsymbol{I}_i\boldsymbol{I}_k) = \sum_{i\neq k} A^{ik}\,(3I_{zi}I_{zk} - \boldsymbol{I}_i\boldsymbol{I}_k) \tag{106}$$

With equations (101) and (102) follows:

$$\boldsymbol{H}_x = \exp\left(-\frac{i}{\hbar}\frac{\pi}{2}I_y\right) H_z \exp\left(\frac{i}{\hbar}\frac{\pi}{2}I_y\right) = \sum_{i\neq k} A^{ik}\,(3I_{xi}I_{xk} - \boldsymbol{I}_i\boldsymbol{I}_k) \tag{107}$$

and

$$\boldsymbol{H}_y = \exp\left(-\frac{i}{\hbar}\frac{\pi}{2}I_x\right) H_z \exp\left(\frac{i}{\hbar}\frac{\pi}{2}I_x\right) = \sum_{i\neq k} A^{ik}\,(3I_{yi}I_{yk} - \boldsymbol{I}_i\boldsymbol{I}_k) \tag{108}$$

Using equations (106) to (108), the averaged Hamiltonian in equation (105) gives:

$$\overline{H} = \frac{1}{3} \sum_{i \neq k} A^{ik} \left[(3 I_{xi} I_{xk} - \boldsymbol{I}_i \boldsymbol{I}_k) + (3 I_{yi} I_{yk} - \boldsymbol{I}_i \boldsymbol{I}_k) + (3 I_{zi} I_{zk} - \boldsymbol{I}_i \boldsymbol{I}_k) \right] = 0 \qquad (109)$$

Solid-state NMR spectroscopy: Experimental techniques / DOR

In contrast to the first-order perturbation of quadrupolar interaction, which has an anisotropic part depending on the geometric term ($3\cos^2\Theta$-1) only (see eq. (38)), the second-order perturbation term describing the line shape of the central transition exhibits a more complicate anisotropic part (see eq. (44)).

Using a representation where p denotes the quantum level p, symmetric coherences with the notation $p/2 \leftrightarrow -p/2$ instead of $m \leftrightarrow -m$ and for the case of fast sample rotation around an axis in the magic angle, the transition $\nu_{p/2,-p/2}$ is given by [Amour1]:

$$\nu_{p/2,-p/2} = \nu_{iso,p} + \nu_{aniso,p} \tag{110}$$

$$= \frac{p\nu_Q^2(3+\eta^2)}{90\nu_0}\left\{I(I+1)-\frac{3}{4}p^2\right\}-\left\{\frac{p\nu_Q^2}{12960\nu_0}\right\}$$
$$\times\left\{(18+\eta^2)d_{0,0}^{(4)}+\sqrt{360}\eta d_{2,0}^{(4)}\cos 2\alpha+\sqrt{70}\eta^2 d_{4,0}^{(4)}\cos 4\alpha\right\}$$
$$\times\left\{36I(I+1)-17p^2-10\right\}\left\{(-\frac{9}{28})\times(35\cos^4\beta-30\cos^2\beta+3)\right\} \tag{111}$$

The Euler angles α and β describe the rotor axis with respect to the principal axis system. $d_{n,0}^{(4)}$ are the reduced Wigner matrices [Rose1].

The anisotropic part in equation (110) disappears if the term with the functions of β in the last bracket of equation (111) is zero, which requires an additional rotation around an axis in an angle of 30.56 or 70.12°.

This average is reached by double-oriented rotation (DOR) using a second inner rotor inside a large outer rotor (see Figure 14).

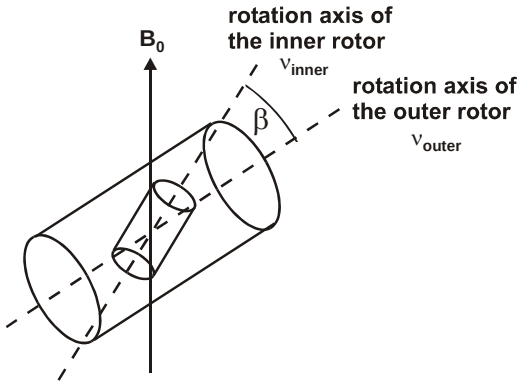

Figure 14
Arrangement of the inner and outer rotor in a DOR NMR probe [Wu1].

Solid-state NMR spectroscopy: Experimental techniques / MQMAS

The multiple-quantum MAS (MQMAS) technique greatly enhances the resolution of spectra due to nuclei with a half-integer spin $I > 1/2$. Basically, this approach combines an excitation of non-observable multiple-quantum transitions {+*m*, -*m*} with the experimentally observed single-quantum transition {+1/2, -1/2} [Frydman1]. The phase development $\varphi(t)$ of a single or multiple-quantum coherence is:

$$\frac{\varphi(t)}{2\pi t} = \Delta\nu \cdot p + \nu_{p/2,-p/2} \tag{112}$$

The first term $\Delta\nu$ includes the chemical shift and the resonance offset:

$$\Delta\nu = \sigma_{iso}\nu_0 - \nu_{offset} \tag{113}$$

The second term of equation (112) corresponds to anisotropic term in equation (111). The multiple-quantum transitions are excited by a single high-power radio frequency pulse (Fig. 15). Subsequently, the multiple-quantum coherence ($p = +m, -m$) is allowed to evolve in t_1. After the evolution period t_1, a second pulse is applied, which converts the multiple-quantum coherences into the coherence $p = -1$. The signal is an echo, which is formed in the time period t_2:

$$t_2 = |QA| \cdot t_1 \tag{114}$$

where *QA* is a term denoting a value of the quadrupolar anisotropy, and causing a refocusing of the anisotopic part. The two-dimensional Fourier transformation of the echo-decays t_2 obtained for different pulse delays t_1 leads to a two-dimensional MQMAS spectrum with featured signals lying along the quadrupolar anisotropy axis δ_2. The isotropic spectrum occurs along the δ_1-axis.

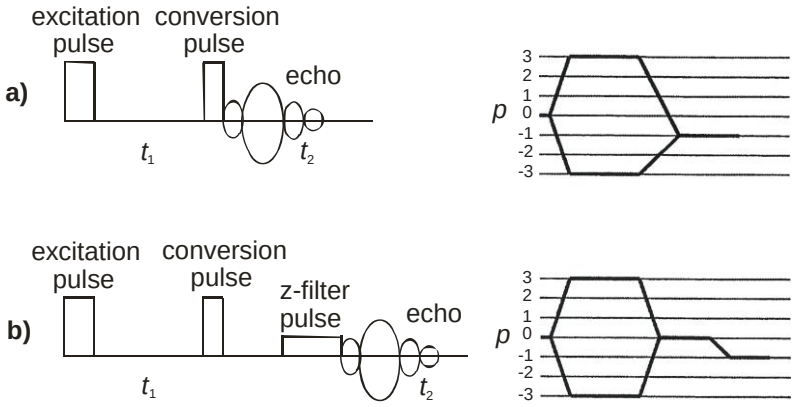

Figure 15

Pulse sequence and coherence transfer pathway of an MQ experiment [Freude1].

Solid-state NMR spectroscopy: Applications

Structures of zeolites:

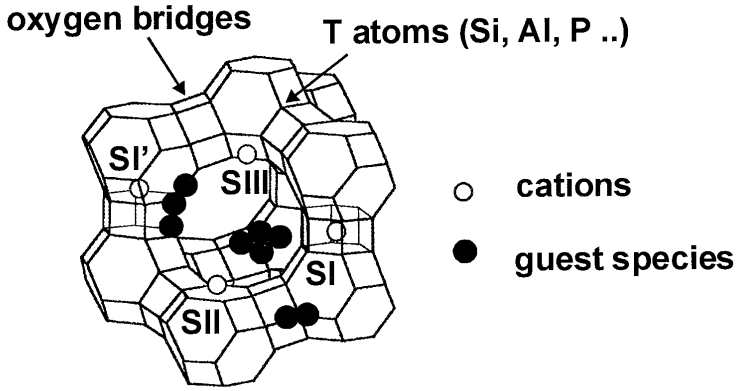

Dependence of the ^{29}Si chemical shifts on the neighbouring T atoms:

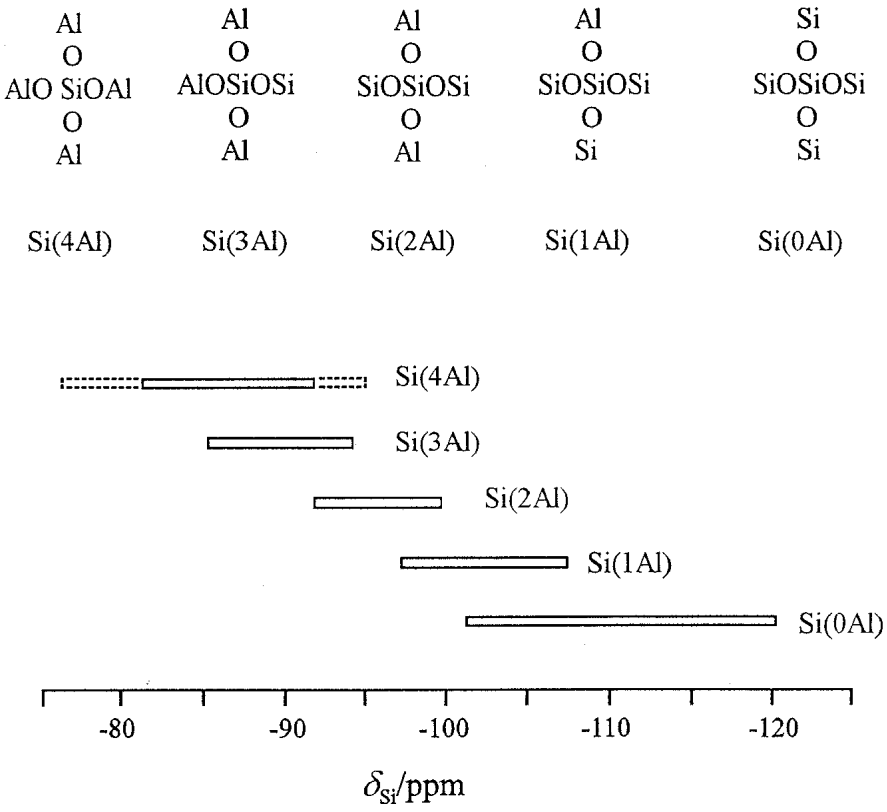

Framework n_{Si}/n_{Al} ratio:

$$n_{Si}/n_{Al} = \sum_{n=0}^{4} I_{Si(nAl)} / \sum_{n=0}^{4} 0.25 \cdot n \cdot I_{Si(nAl)}$$

Solid-state NMR spectroscopy: Applications

^{29}Si MAS NMR spectra of different aluminium-containing zeolites (top) and of their highly siliceous (bottom) forms [Thom1]:

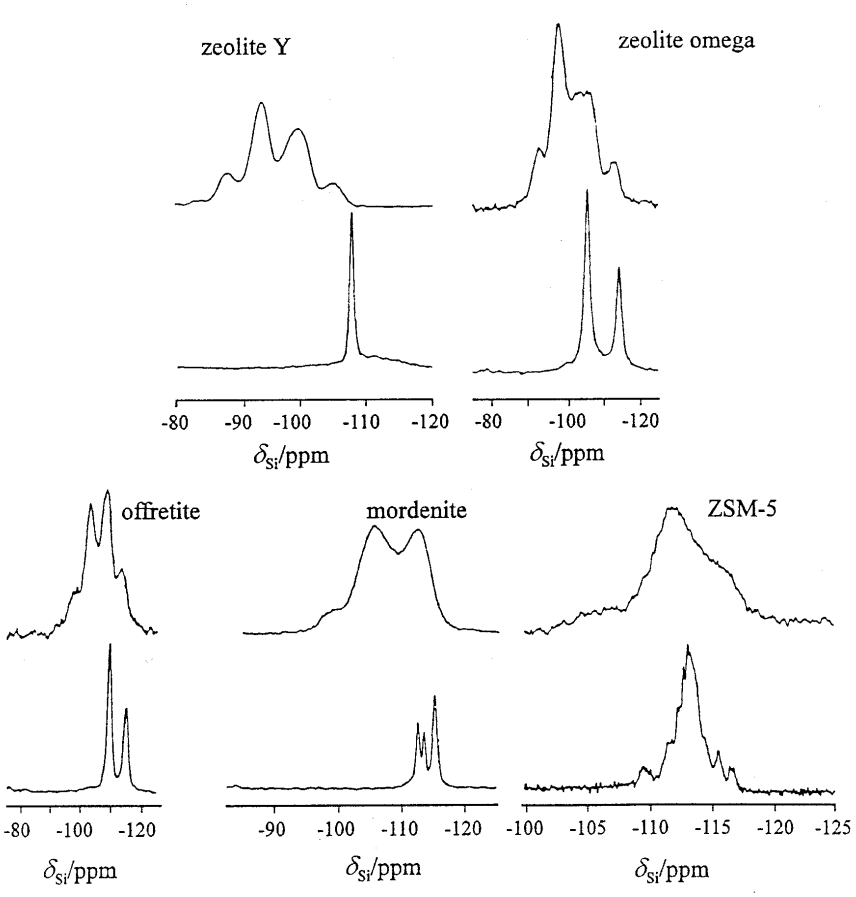

Table of ^{29}Si chemical shifts of Si(nAl) units in some selected zeolites [Karg1]:

zeolite	n_{Si}/n_{Al}	Site	Si(4Al)	Si(3Al)	Si(2Al)	Si(1Al)	Si(0Al)
Y	2.5	T	-83.8	-89.2	-94.5	-100.0	-105.5
	∞	T					-107.8
Omega	3.1	T1		-89.1	-93.7	-98.8	-103.4
		T2	-89.1	-93.7	-98.8	-107.0	-112.0
	∞	T1					-106.0
		T2					-114.4
mordenite	5.0	T1 to T4			-100.1	-105.7	-112.1
	∞	T1					-112.2
		T4					-113.1
		T2 + T3					-115.0
ZSM-5	20	T1 to T12				-106.0	-112.0

Solid-state NMR spectroscopy: Applications

Influence of the mean T-O-T angle α on the ^{29}Si chemical shift [Engel1]:

$$\delta_{29Si} / \text{ppm} = -5.230 - 0.570\ \alpha \quad (115)$$

$$\delta_{29Si} / \text{ppm} = -223.9 \cdot \cos\alpha/(\cos\alpha - 1) + 5n - 7.2 \quad (116)$$

with the number *n* of aluminium atoms in the second coordination sphere.

Experimental (top) and calculated (bottom) ^{29}Si MAS NMR spectrum of siliceous zeolite ZSM-5 with 24 different T positions [Engel2]:

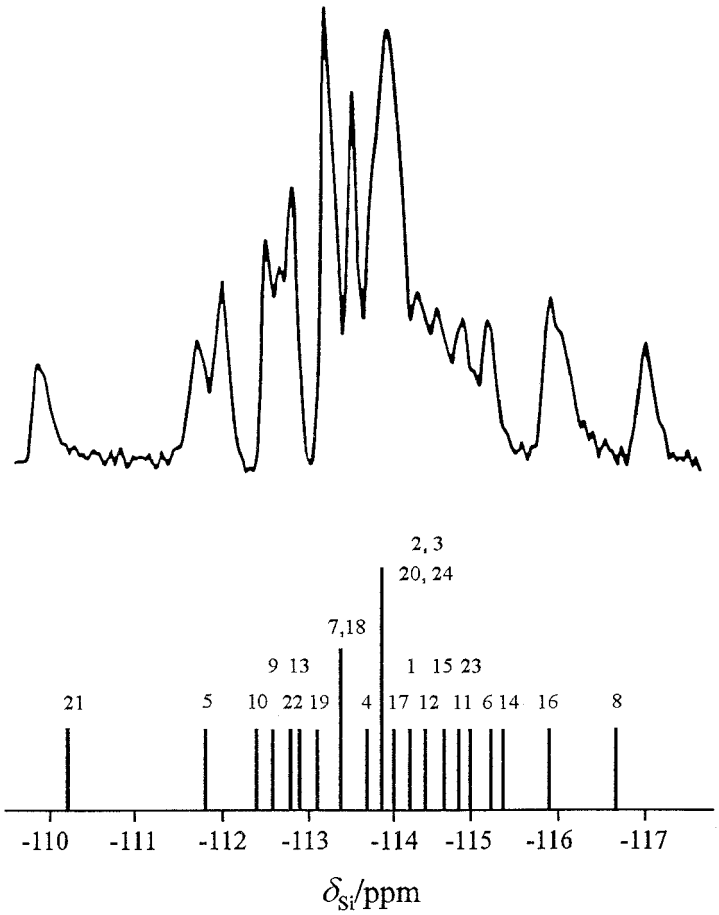

Solid-state NMR spectroscopy: Applications

Study of the connectivities of silicon atoms in zeolite ZSM-39 by sampling the J-coupling (ca. 1–10 Hz) with the two-dimensional ^{29}Si COSY MAS NMR experiment [Fyfe1]:

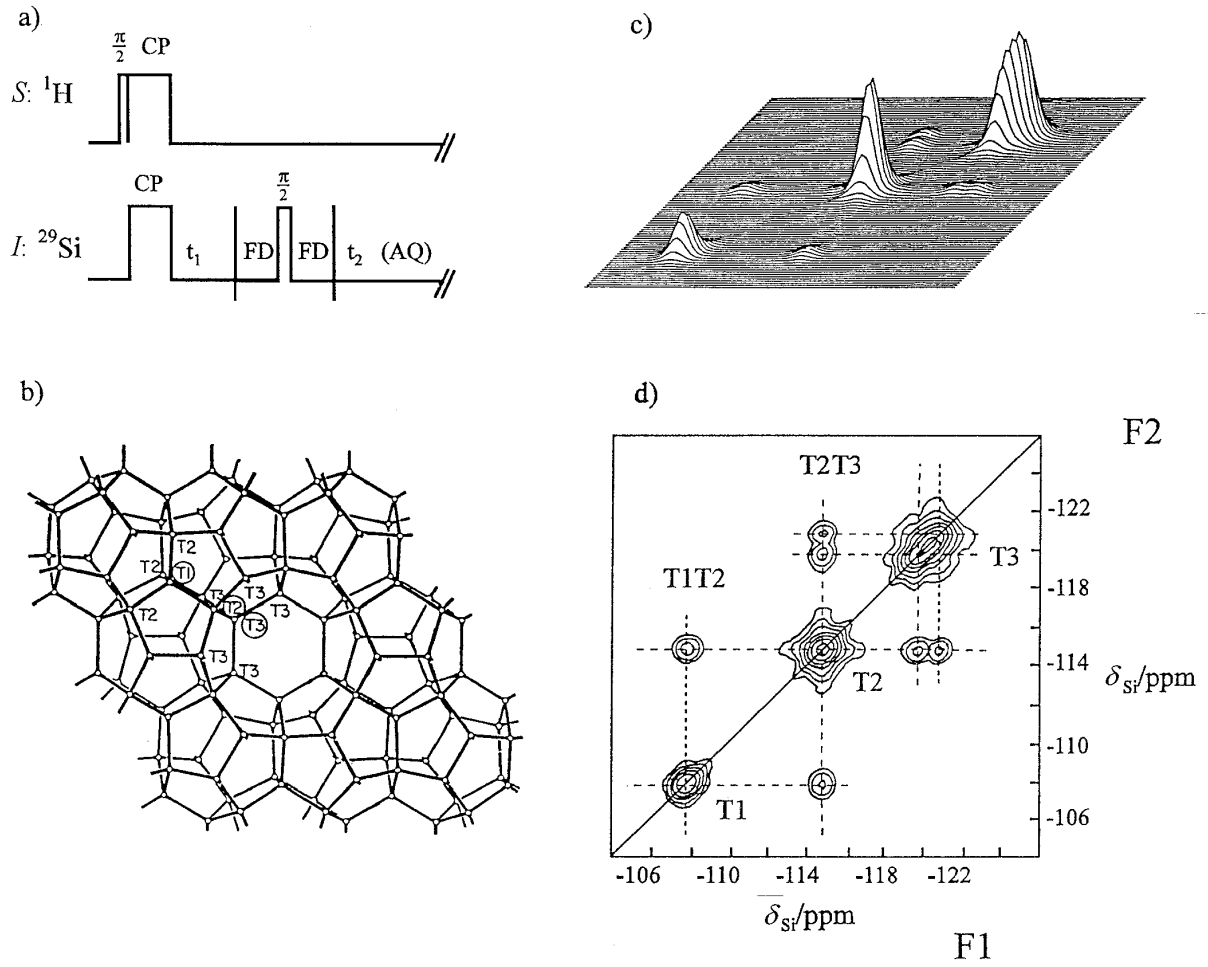

a) pulse sequence (parameter FD is a fixed delay of 5 ms)
b) zeolite structure with T positions
c) 2D COSY MAS NMR spectrum (stacked plot)
d) 2D COSY MAS NMR spectrum (contour plot)

Solid-state NMR spectroscopy: Applications

^{27}Al MAS NMR of crystalline aluminosilicates (zeolite H-Y) containing tetrahedrally (Al^{IV}) and octohedrally (Al^{VI}) coordinated aluminum [Rocha1]:

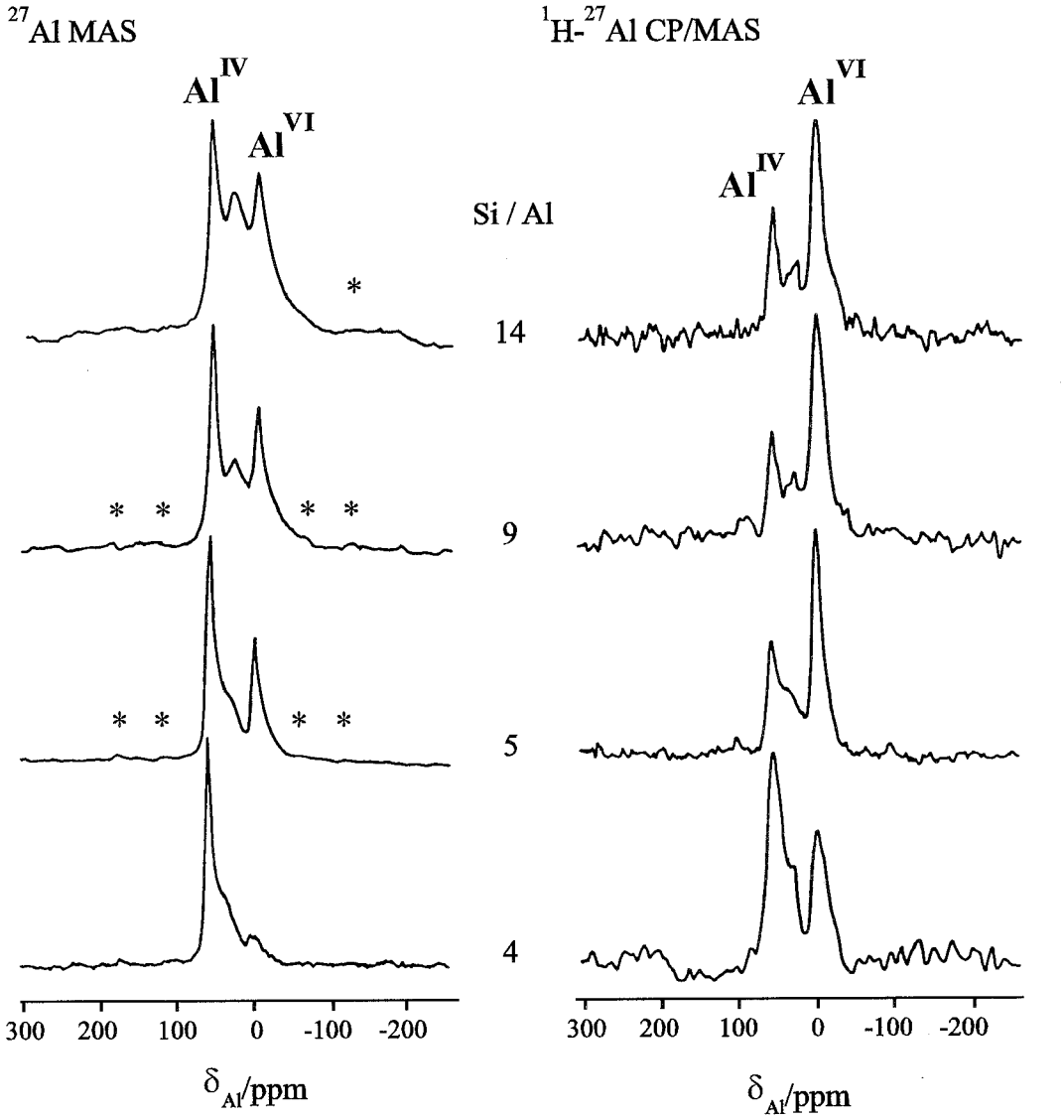

CP raises the intensities of signals due to atoms interacting with water molecules (hexa-aquo complexes, extra-framework aluminum).

Solid-state NMR spectroscopy: Applications

^{1}H MAS NMR spectroscopy of hydroxyl groups in zeolite Y (SiOH: ca. 1.8 ppm, SiOHAl: 3.9 to 4.2 ppm, MeOH: -0.5 to 5.6 ppm,) exchanged with different cations (a-c) and after dealumination (d) [Hung1]:

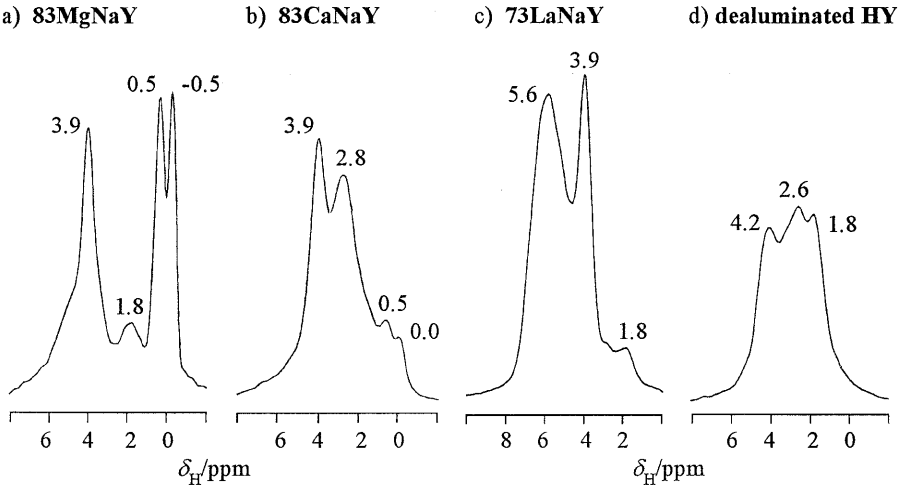

Scheme of a NOESY NMR experiment sampling spin diffusion during Δ:

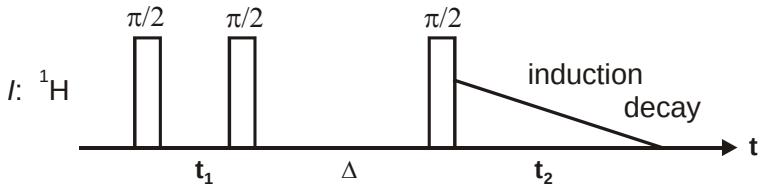

Contour plots of ^{1}H NOESY MAS NMR experiments performed with dehydrated silicoaluminophosphate SAPO-5 and zeolite HZSM-5 [Hung1]:

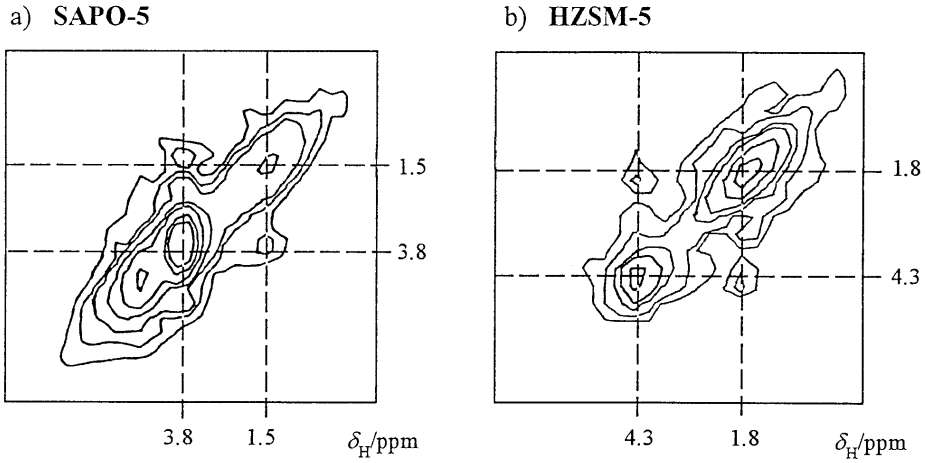

Cross peaks indicate spin diffusion between defect SiOH groups at 1.5 to 1.8 ppm and bridging OH groups at 3.8 to 4.3 ppm.

Solid-state NMR spectroscopy: Applications

Equipment for the preparation of solid catalysts for in situ MAS NMR investigations of surface sites and adsorbate complexes [Munson1, Zhang1]:

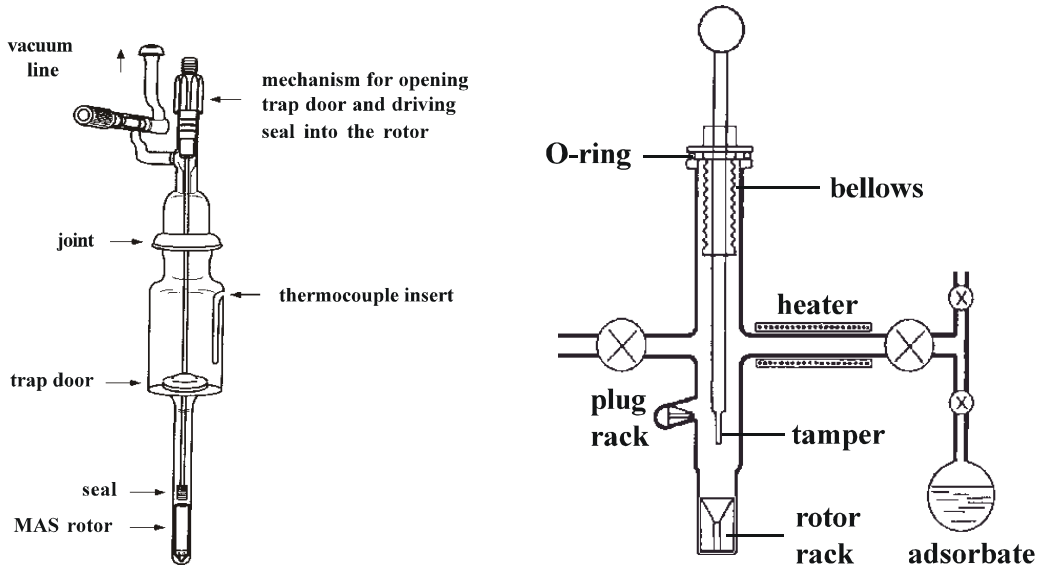

Scheme of a Laser heating system in a high-temperature MAS NMR probe [Mild1]:

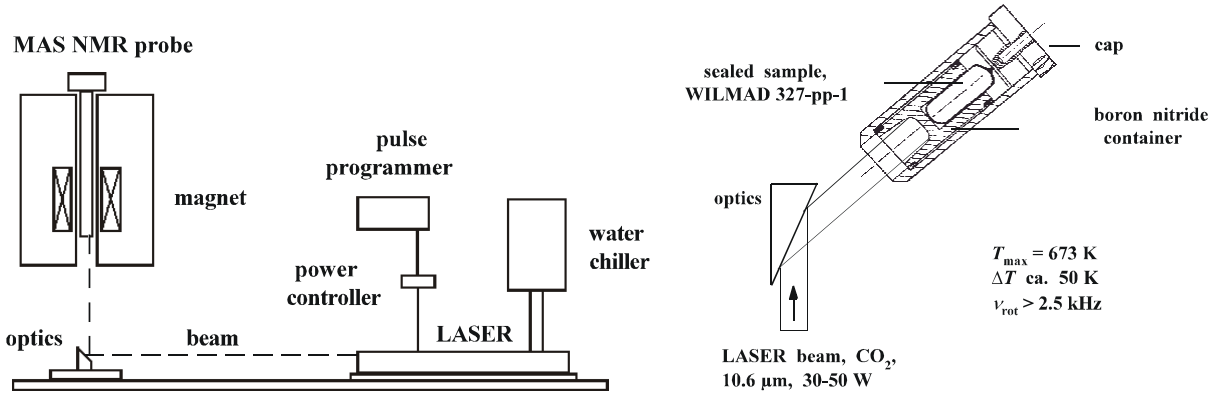

Temperatures up to 923 K at rotation frequencies of up to 3.5 kHz can be reached.

Because of Curie's law:

$$M_0 = \frac{N\gamma^2\hbar^2 I(I+1)B_0}{3k_B T} \qquad (117)$$

the magnetization and decrease with increasing temperature T, which can be a limitation for NMR spectroscopy under in situ conditions.

Solid-state NMR spectroscopy: Applications

Studies of reactions catalyzed by surface sites of microporous solids such as nitration of toluene with nitric acid and acetic anhydride on zeolite H-Beta [Hao1]:

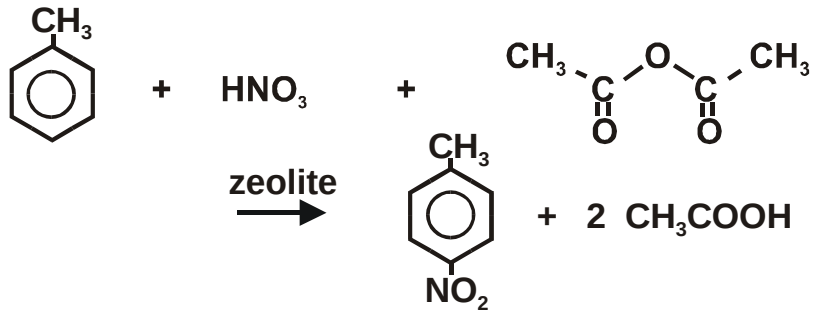

^{27}Al MAS NMR of octahedrally (Al^{VI}) and tetrahedrally (Al^{IV}) coordinated aluminium in zeolite H-Beta and ^{15}N MAS NMR of reactants [Hao1]:

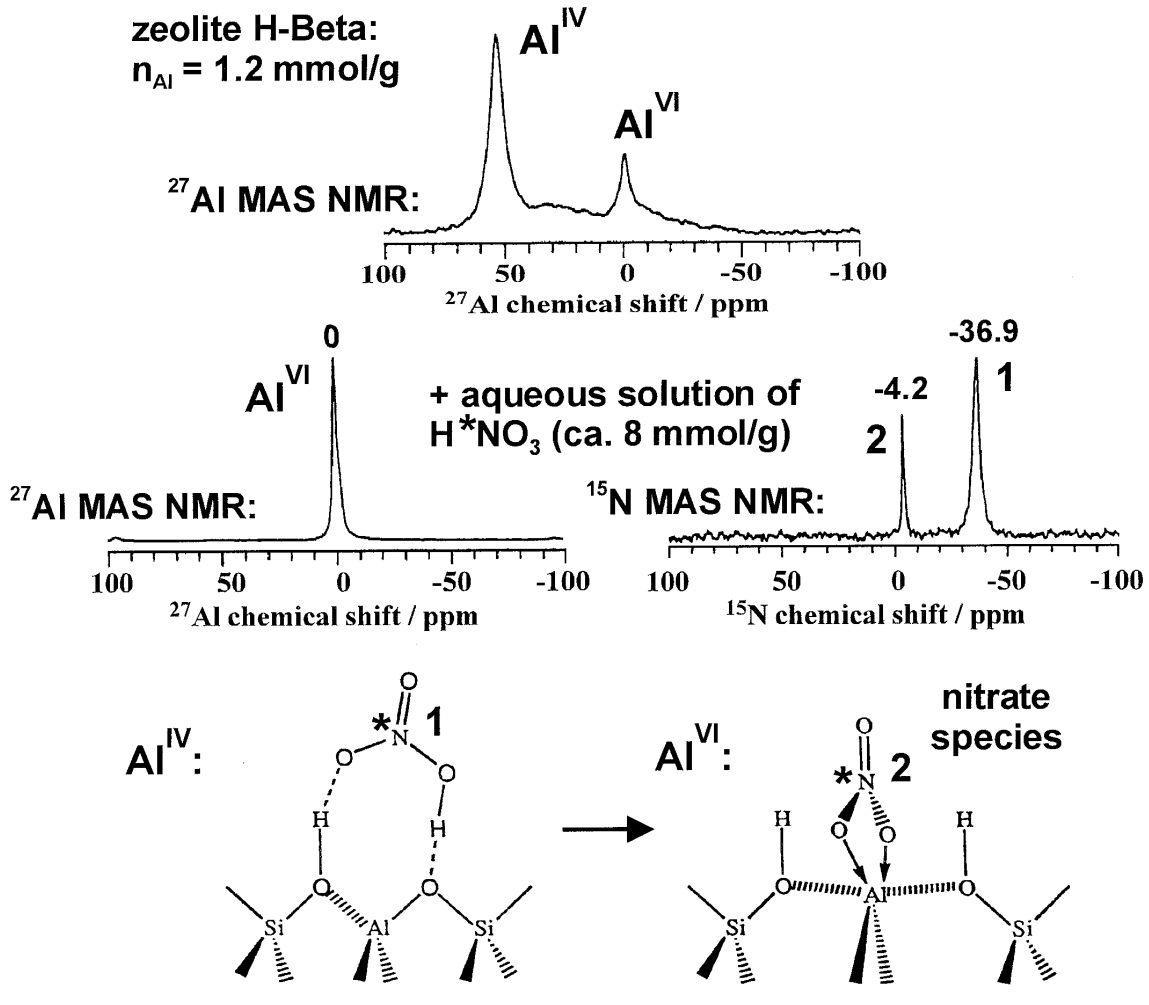

Solid-state NMR spectroscopy: Applications

Continuation of nitration of toluene with nitric acid and acetic anhydride on zeolite H-Beta [Hao1]:

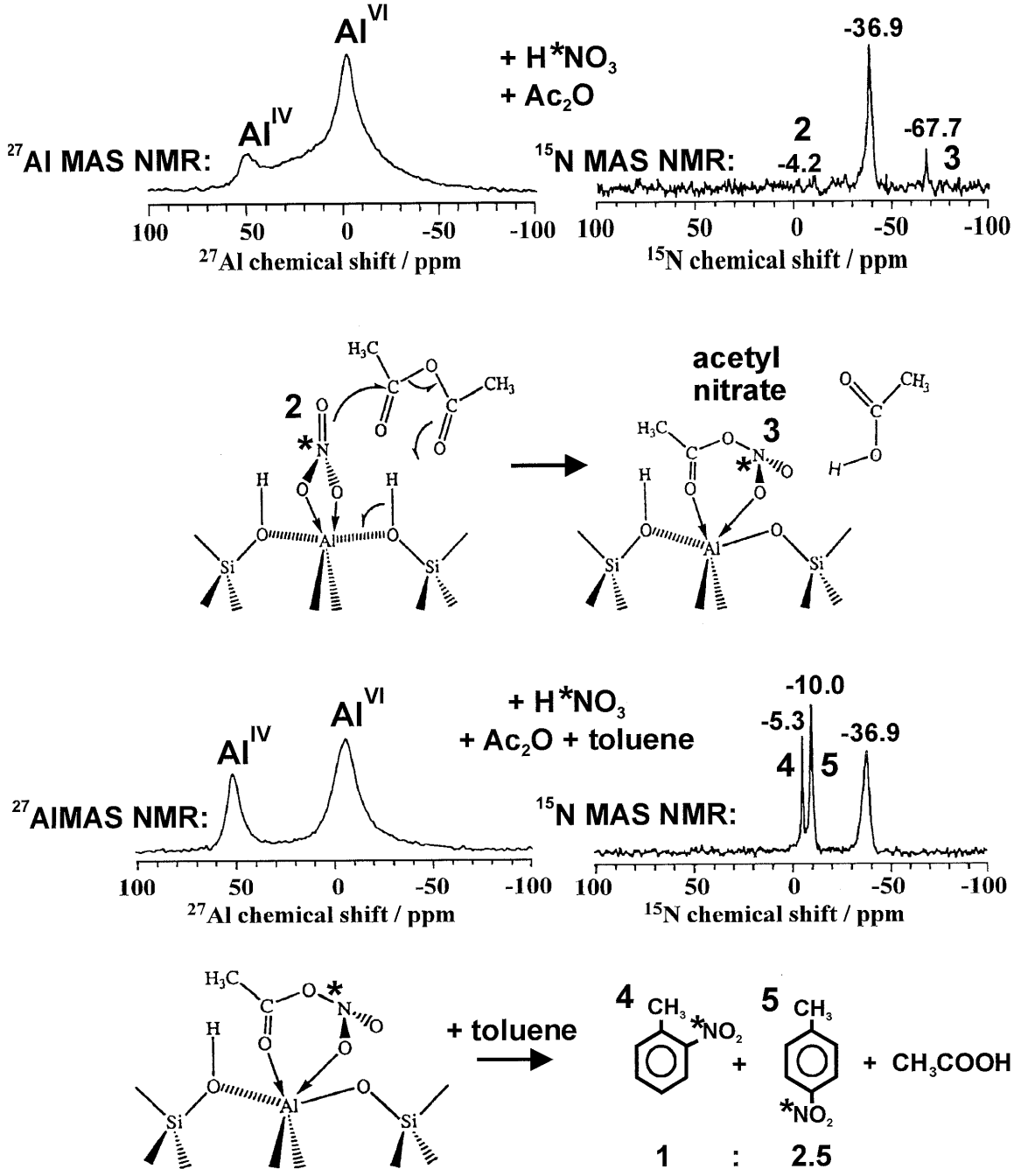

Solid-state NMR spectroscopy: Applications

Double resonance pulse sequences for the investigation of bond geometries [Smith]:

SEDOR (Spin Echo DOuble Resonance)

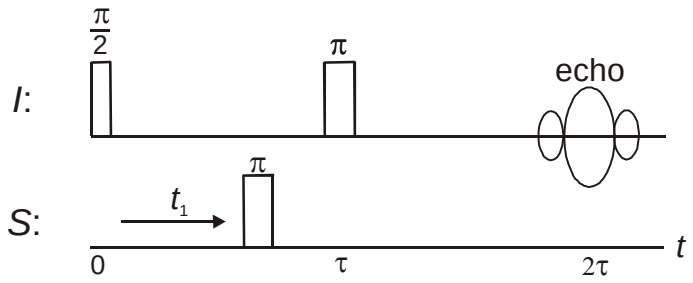

The experiment is performed without application of MAS. During the first pulse delay of a $\pi/2$-τ-π-τ echo sequence applied to the spins *I*, a single π-pulse is applied to the spins *S*. This π-pulse inverts the sign of the dipolar coupling, which perturbs the dipolar refocusing process and diminishes the echo intensity for coupled spin pairs *I*-*S*.

SEDOR fraction:

$$S_f(t_1) = \frac{S_0 - S(t_1)}{S_0} \tag{118}$$

with

$$S(t_1) = \int_0^{\pi} \cos\left[D t_1 (3\cos^2\theta - 1)\right] \cdot \sin\theta \cdot d\theta \tag{119}$$

Here, $D = \gamma_I \gamma_S \hbar / r_{IS}^3$, r_{IS} defines the distance between the coupled spins *I* and *S*, and θ is the angle between the internuclear vector r_{IS} and the external magnetic field B_0. S_0 is the echo intensity without application of the π-pulse to the spin *S* ensemble. As an example, SEDOR was used to determine the Al-P distance in the aluminophosphate $AlPO_4$-5. A fitting of the SEDOR curve led to D = 405 ± 10 Hz corresponding to $r_{Al,P}$ = 315 ± 3 pm [Eck2].

Solid-state NMR spectroscopy: Applications

REDOR (Rotational Echo DOuble Resonance)

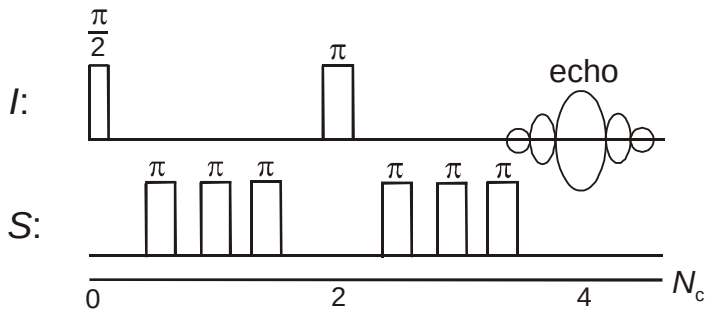

Is in principle a SEDOR experiment in combination with MAS. A rotor synchronised echo sequence is applied to the spins *I*, which are detected after a time 2τ equalling an even number N_c of rotation periods. For decoupling the dipolar interaction between the spins *I* and *S*, π-pulses are applied to the spin *S* ensemble at every half rotation period T_r. The dipolar coupling is obtained by measuring the REDOR fraction, which describes the loss of the echo intensity as a function of the number of rotor periods:

$$\frac{S_0 - S(N_c T_r)}{S_0} = \frac{1}{\pi^2 S(S+1)} (N_c T_r)^2 M_{2,\mathrm{IS}} \qquad (120)$$

$M_{2,\mathrm{IS}}$ is the second moment of the heteronuclear dipolar interaction given in Equation (68). This term contains r_{IS}, which is the distance between the coupled spins *I* and *S*. Again, S_0 is the echo intensity obtained without application of π-pulses to the spin *S* ensemble.

As an example, zeolite H-Beta dealuminated by ammonium hexafluorosilicate was investigated with REDOR [Kao1]. The REDOR fraction of the signal of extra-framework aluminium atoms at 0 ppm gave a dipolar coupling constant corresponding to an Al-F distance of 180 to 220 pm. This finding indicates that the aluminum atoms occurring in extra-framework clusters of the dealuminated zeolite H-Beta under study are directly bound to fluorine atoms.

Solid-state NMR spectroscopy: Applications

TRAPDOR (TRAnsfer of Population in DOuble Resonance)

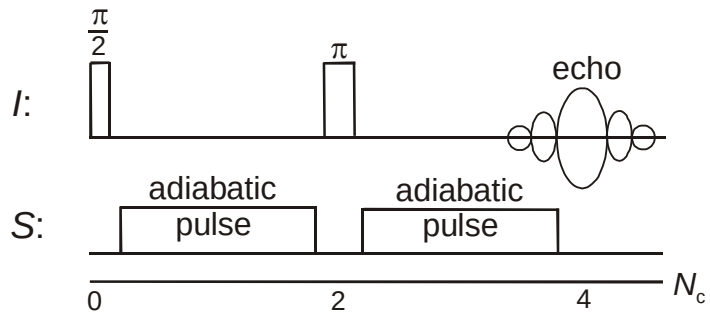

The TRAPDOR and REAPDOR experiments were designed specifically for the study of spins *I* interacting with quadrupolar nuclei having the spin $S > 1/2$. In the TRAPDOR experiment, a rotor synchronized echo sequence is applied to the spins *I*. During the pulse and echo delay, the quadrupolar nuclei with spin *S* are continuously irradiated, which leads in combination with MAS leads to rotationally induced level transitions. Since these level transitions are difficult to calculate, TRAPDOR is a qualitative experiment only.

REAPDOR (Rotational Echo Adiabatic Passage Double Resonance)

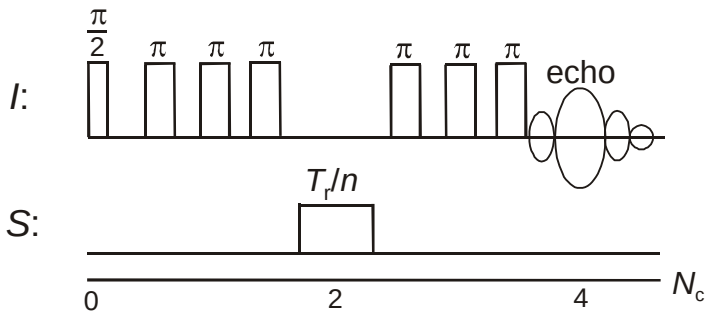

In contrast to TRAPDOR, a train of rotor synchronized π-pulses is applied on the spins *I* at every half rotation period T_r. In the first half of the evolution period, the spins *I* will dephase as a result of the chemical shift anisotropy and the heteronuclear dipolar coupling. In the second half of the evolution period, the magnetization is refocused and an echo is formed. In the center of the evolution period, a so-called adiabatic passage pulse is applied to the spins *S*. (duration of $T_r/3$ to $T_r/2$). The dipolar dephasing of the spins *I*, which are coupled with spins *S*, can not be refocused in the echo and an decrease of the echo intensity occurs. The quantitative evaluation of the REAPDOR fraction is performed similar to the REDOR fraction. REAPDOR has been employed to study the local structure of silicon atoms in the framework of the aluminum substituted molecular sieve ETS-10 [Gana1].

Solid-state NMR spectroscopy: Applications

^{27}Al-^{31}P correlation MAS NMR spectrum of the aluminophosphate VPI-5 [Eck1]:

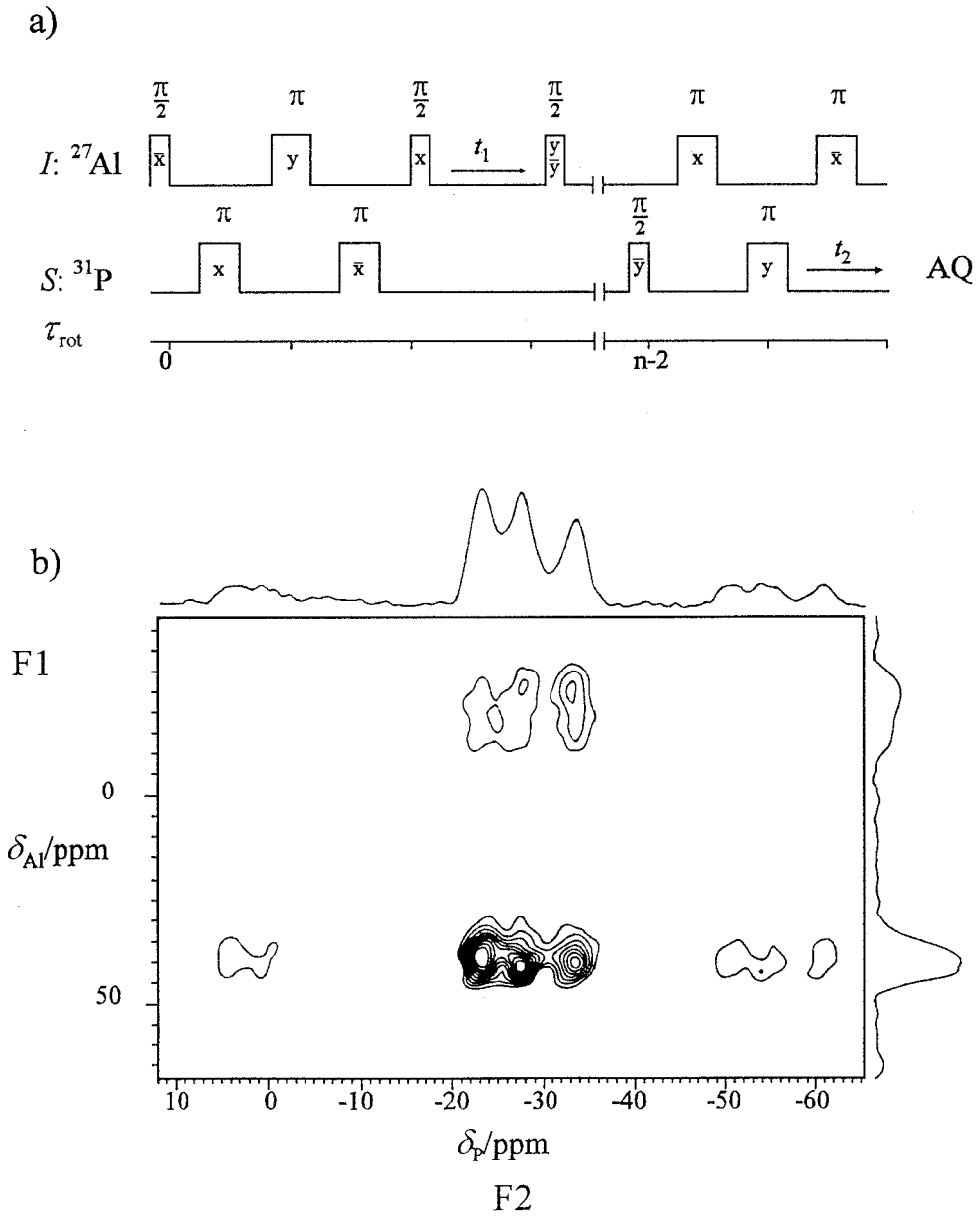

a) double resonance pulse experiment consisting of REDOR (rotational-echo double resonance) sequences
b) 2D spectrum (contour plot)

The experiment indicates a coupling of all phosphorus atoms with tetrahedrally coordinated framework aluminium.

Solid-state NMR spectroscopy: Applications

Scheme of a DOR (double oriented rotation) rotor:

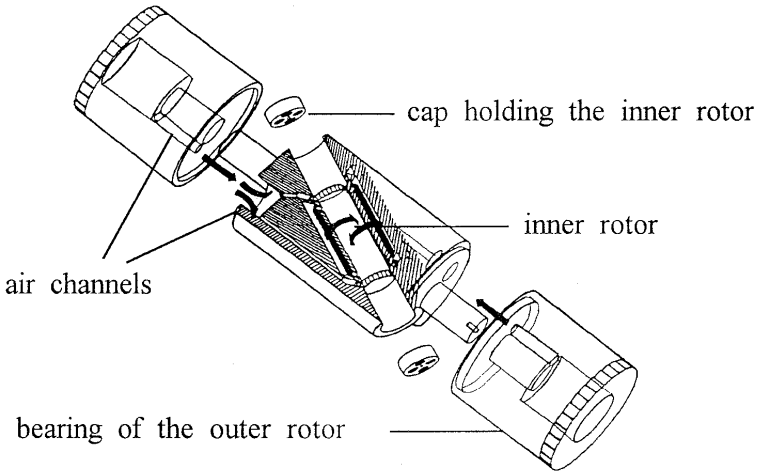

Suppression of sidebands caused by the outer DOR rotor (^{23}Na DOR NMR of Na_2SO_4, $\nu_{rot,outer}$ = 650 Hz):

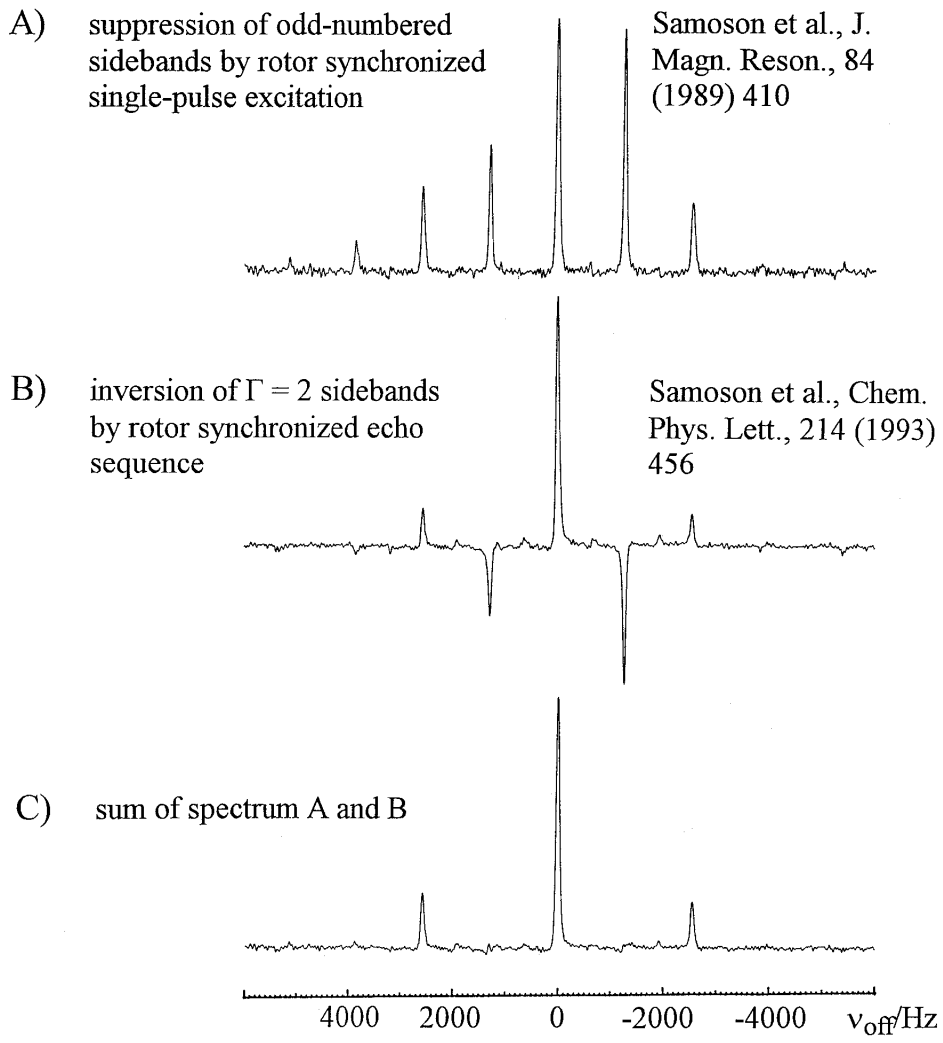

Solid-state NMR spectroscopy: Applications

Comparison ^{23}Na static, MAS, and DOR NMR spectroscopy of sodium cyclotriphosphate $Na_3P_3O_9$:

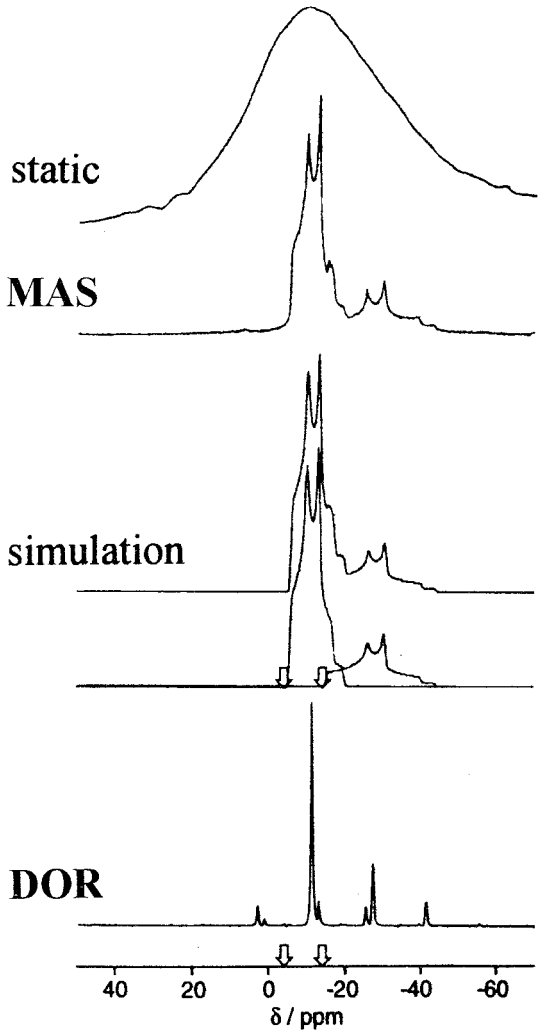

solid-state line broadening by: $H_D + H_{CS} + H_Q^{(1)} + H_Q^{(2)}$

$H_Q^{(2)}$

total averaging of solid-state interactions

Results of simulation:

parameter	Na_1	Na_2
QCC	2.2 MHz	1.6 MHz
η	0.7	0.55
δ_{iso}	–14.8 ppm	–5.6 ppm

Solid-state NMR spectroscopy: Applications

Local structure of sodium cations in dehydrated zeolite Na-Y:

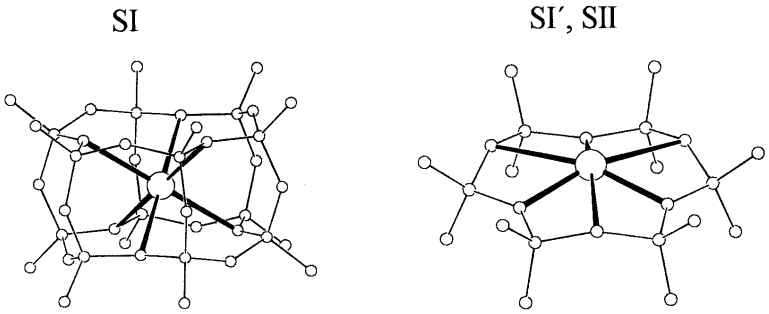

QCC = 0-0.5 MHz ⇓ low-field line A corresponds to SI

QCC = 3.4-5.6 MHz ⇓ high-field pattern B corresponds to SI′ and SII

^{23}Na MAS NMR (left) and 2D ^{23}Na nutation MAS NMR spectrum of dehydrated zeolite Na-Y [Hung2]:

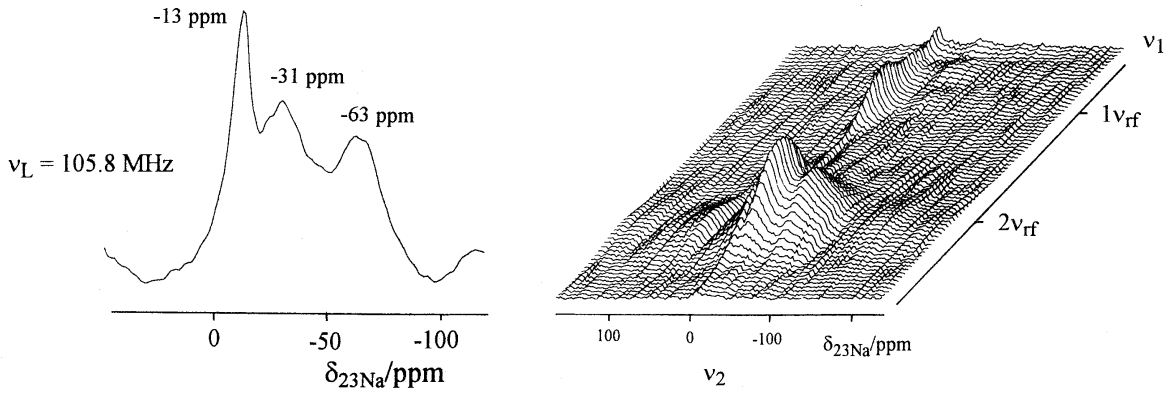

Scheme of the 2D nutation NMR experiment:

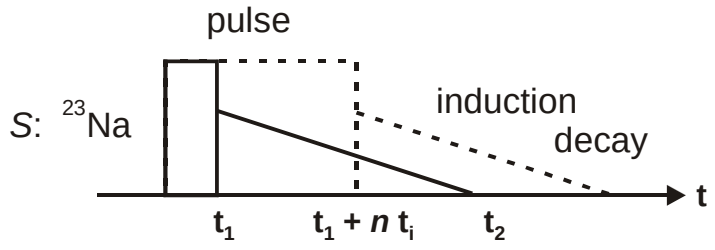

Solid-state NMR spectroscopy: Applications

^{23}Na DOR NMR spectra of dehydrated zeolite Na-Y in different magnetic fields (left and right) and recorded with different sample spinning frequencies (top to bottom) [Hung2]:

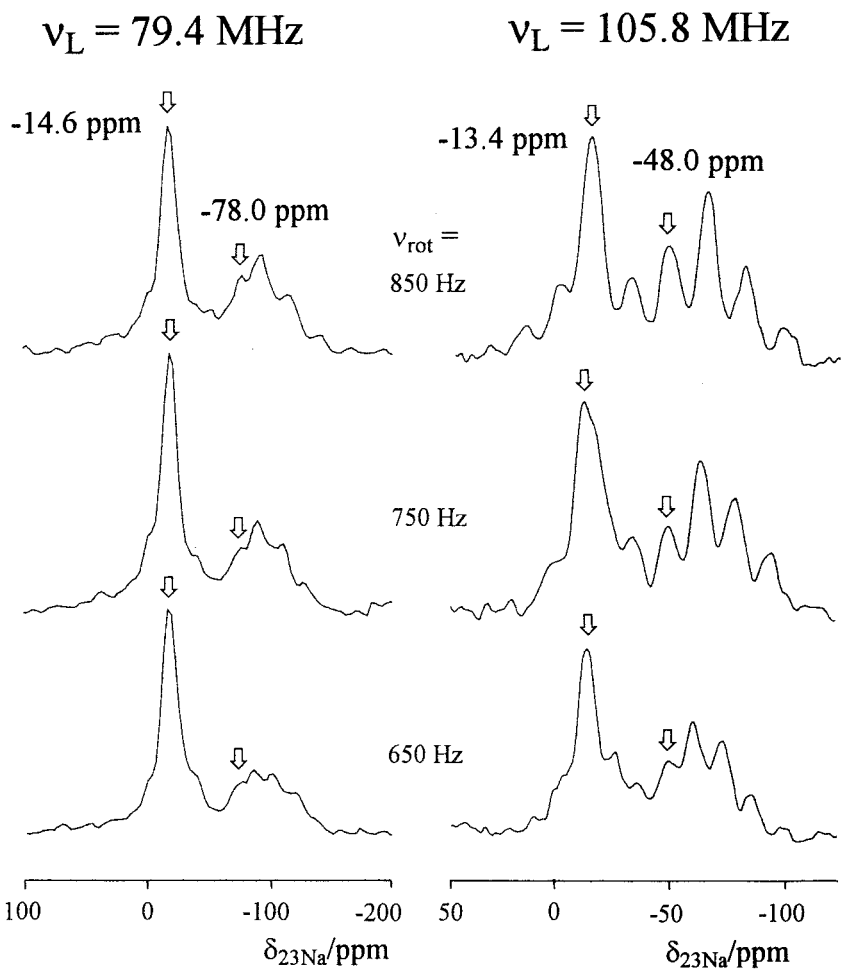

$$\delta_{iso} = \frac{\delta_1^{DOR} K_2 - \delta_2^{DOR} K_1}{K_2 - K_1} \quad \Longrightarrow \quad \text{isotropic chemical shift} \tag{121}$$

$$K_n = \frac{3 \cdot 10^6 [I(I+1) - 3/4]}{40 \nu_{Ln}^2 I^2 (2I-1)^2} \tag{122}$$

$$\overline{QCC}^* = \sqrt{\frac{\delta_1^{DOR} - \delta_2^{DOR}}{K_2 - K_1}} \quad \Longrightarrow \quad \text{quadrupole coupling constant} \tag{123}$$

Solid-state NMR spectroscopy: Applications

A suitable tool for the discussion of the value of quadrupolar coupling constants of ^{27}Al nuclei in AlO_4 tetrahedra is the shear strain parameter $|\Psi|$:

$$|\Psi| = \sum_{i=1}^{6} |\tan(\Theta_i - \Theta_0)| \qquad (124)$$

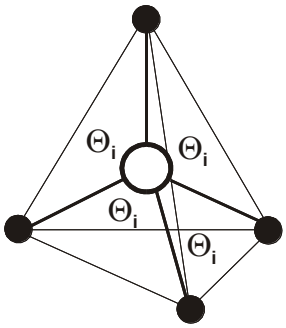

Schematic drawing (top) of the structure of the aluminophosphate VPI-5 and correlation of the quadrupolar coupling constant C_q of ^{27}Al nuclei as a function of the shear strain parameter $|\Psi|$ of AlO_4 tetrahedra in aluminate sodalites (△, ▽), feldspars (□), and VPI-5(●) [Karg1]:

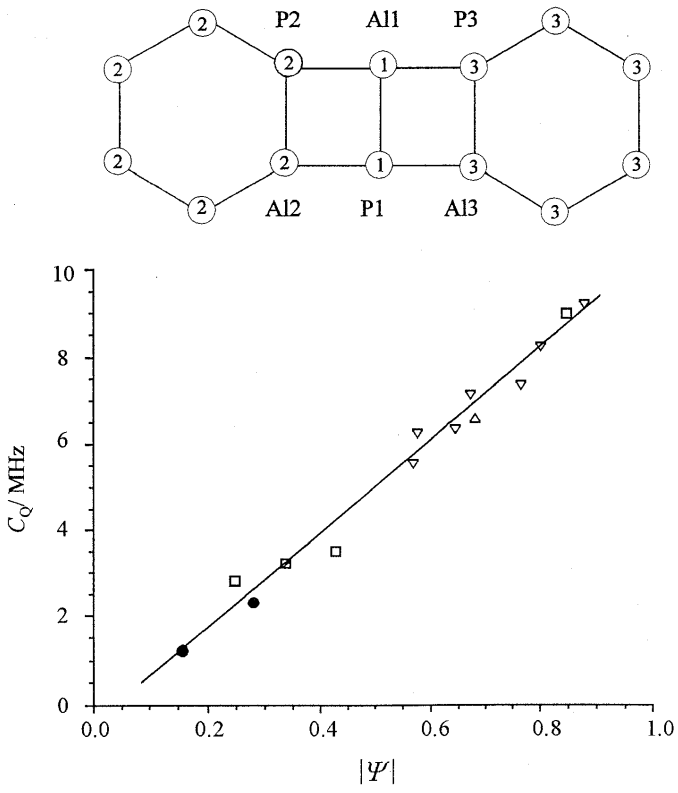

Solid-state NMR spectroscopy: Applications

^{17}O 3QMAS NMR spectra of zeolite Na-ZSM-5 after the 2D Fourier transformation (left) and after the shearing transformation (right) [Freude1]:

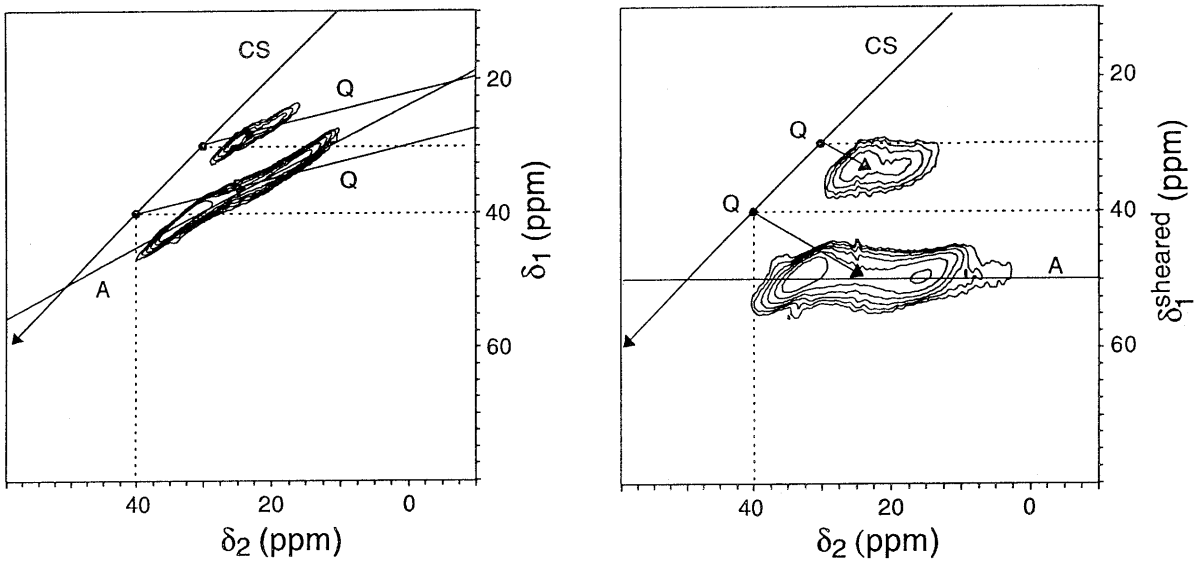

The spectra consist of signals due to SiOSi (80%, C_Q = 5.3 MHz) and SiOAl (20%, C_Q = 3.5 MHz) bridges.

Before shearing, the chemical shifts along the two dimensions are given by [Amour2]:

$$\delta_1 = \delta_{\text{iso}} + \delta_{\text{qs}} = \delta_{\text{iso}} - \frac{\nu_{\text{Q}}^2\left(3+\eta^2\right)\left[4I(I+1)-3p^2\right]}{360\nu_0^2} \tag{125}$$

and

$$\delta_2 = \delta_{\text{iso}} + \delta_{qs} = \delta_{\text{iso}} - \frac{\nu_{\text{Q}}^2\left(3+\eta^2\right)\left[4I(I+1)-3\right]}{360\nu_0^2}. \tag{126}$$

with the isotropic chemical shift δ_{iso} and the second-order quadrupolar shift δ_{qs}.

The shearing modifies shift values along the ν_1 axis according to [Amour2]:

$$\delta_1^{\text{shearing}} = \delta_{\text{iso}} + \delta_{\text{qs}}^{\text{shearing}} = \delta_{\text{iso}} + \frac{\nu_{\text{Q}}^2 \left(3+\eta^2\right)\left[4I\left(I+1\right)-3\right]}{612\nu_0^2}. \qquad (127)$$

Solid-state NMR spectroscopy: Literature

[Abra1] A. Abragam, Principles of Nuclear Magnetism, Oxford Science Publications, 1994.

[Amour1] J.P. Amoureux, Solid State NMR 2 (1993) 83.

[Amour2] J.P. Amoureux, C. Fernandez, Solid State Nucl. Magn. Reson. 10 (1998) 211.

[Andrew1] E.R. Andrew, A. Jasinski, J. Phys. C 4 (1971) 391.

[Dixon1] W.T. Dixon, J. Chem. Phys. 77 (1982) 1800.

[Eck1] E.R.H. van Eck, W.S. Veeman, J. Am. Chem. Soc. 115 (1993) 1168.

[Eck2] E.R.H. van Eck, W.S. Veeman, Solid State Nucl. Magn. Reson. 1 (1992) 1.

[Engel1] G. Engelhardt, M. Michel, High-Resolution Solid-State NMR of Silicates and Zeolites, Wiley, Chichester, New York, 1987.

[Engel2] G. Engelhardt, H. van Koningsveld, Zeolites 10 (1990) 650.

[Fraiss1] J. Fraissard, R. Vincent, C. Doremieux, J. Kärger, H. Pfeifer, Application of NMR Methods to Catalysis, in: Catalysis, Science and Technology, J.R. Anderson, M. Boudart (eds.), Springer-Verlag, Berlin, Heidelberg, 1996, pp. 1-176.

[Freude1] D. Freude, Quadrupolar Nuclei in Solid-state Nuclear Magnetic Resonance, in: Encylopedia of Analytical Chemistry, R.A, Meyers (Ed.), Wiley, New York, Chichester, 2000, pp. 12188-12224.

[Freude2] D. Freude, J. Haase, Quadrupolar Effects in Solid-state NMR, Basic Principles and Progress, Vol. 29, Springer-verlag, Berlin, Heidelberg, 1993, pp. 1-90.

[Frydman1] L. Frydman, J.S. Harwood, Isotropic Spectra of Half-integer Quadrupolae Spins from Bidimensional Magic-angle Spinning NMR, J. Am. Chem. Soc. 117 (1995) 5367.

[Fyfe1] C.A. Fyfe, H. Gies, Y. Feng, J. Am. Chem. Soc. 111 (1989) 7702.

[Gana1] S. Ganapathy, R. Kumar, V. Montouillout, C. Fernandez, J.P. Amoureux, Chem. Phys. Lett. 390 (2004) 79.

[Grimmer1] A.-R. Grimmer, B. Blümich, Introduction to Solid-state NMR, in: Solid-state NMR II – Iorganic Matter, NMR Basic Principles and Progress, Vol. 30, Springer-Verlag, Berlin, Heidelberg, 1994, pp. 1-62.

[Hao1] M. Haouas et al., Catal. Lett. 70 (2000) 61.

[Hung1] M. Hunger, Catal.-Rev.-Sci. Eng. 39 (1997) 345.

[Hung2] M. Hunger, G. Engelhardt, H. Koller, J. Weitkamp, Solid State Nucl. Magn. Reson. 2 (1993) 111.

[Kao1] H.-M. Kao, Y.-C. Chen, J. Phys. Chem. B 107 (2003) 3367.

[Karg1] H.G. Karge, M. Hunger, H.K. Beyer, in J. Weitkamp, L. Puppe, Catalysis and Zeolites, Springer-Verlag, Berlin, Heidelberg, 1999.

[Michel1] D. Michel, F. Engelke, NMR Basic Principles and Progress, Vol. 32, Springer-Verlag, Berlin, Heidelberg, 1995, pp. 69-125.

[Mild1] T. Mildner et al., J. Am. Chem. Soc. 119 (1997) 4258.

[Munson1] E.J. Munson et al., J. Catal. 136 (1992) 504.

[Pfeifer1] H. Pfeifer, NMR Basic Principles and Progress, Vol. 31, Springer-Verlag, Berlin, Heidelberg, 1994, pp. 32-90.

Solid-state NMR spectroscopy: Literature

[Rocha1] J. Rocha, S.W. Carr, J. Klinowski, Chem. Phys. Lett. 187 (1991) 401.
[Rose1] M.E. Rose, Elementary Theory of Angular Momentum, Wiley, New York, Chichester, 1967.
[Samo1] A. Samoson, Satellite Transition High-resolution NMR of Quadrupole Nuclei in Powders, Chem. Phys. Lett. 85 (1985) 29-32.
[Smith] M.E. Smith, E.R.H. van Eck, Progr. Nucl. Magn. Reson. 34 (1999) 159.
[Thom1] J.M. Thomas, J. Klinowski, S. Ramdas, B.K. Hunter, D.T.B. Tennakoon, Chem. Phys. Lett. 102 (1983) 158.
[Wu1] Y. Wu, B.Q. Sun, A. Pines, A. Samoson, E. Lippmaa, NMR Experiments with a New Double Rotor, J. Magn. Reson. 89 (1990) 297.
[Zhang1] W. Zhang et al., Chem. Commun. (1999) 1091.